ELSEVIER

Quaternary Science Reviews 24 (2005) 1499–1520

QSR

Provenance of LGM glacial till (sand fraction) across the Ross embayment, Antarctica

Kathy J. Licht*, Jason R. Lederer, R. Jeffrey Swope

Department of Geology, Indiana University– Purdue University Indianapolis, Indianapolis, IN 46202, USA

Received 21 June 2004; accepted 15 October 2004

Abstract

The provenance of Late Quaternary Ross Embayment till was investigated by comparing the coarse sand composition of East and West Antarctic source area tills with till samples from across the Ross Sea. The West Antarctic samples from beneath the Whillans (B) and Kamb (C) ice streams are petrologically distinct from samples of lateral moraines flanking several East Antarctic outlet glaciers. The characteristic assemblage of four West Antarctic samples includes felsic intrusive and detrital sedimentary lithic fragments, plagioclase and abundant quartz. In contrast, most of the ten East Antarctic till samples contains abundant mafic intrusive and detrital sedimentary lithic fragments as well as less abundant quartz. The distinctive composition of these source areas can be linked to 33 samples from 20 cores of Last Glacial Maximum (LGM) age till distributed across the Ross Sea. Western Ross Sea till samples exhibit mineralogic and lithological similarities to East Antarctic till samples, although these western Ross Sea tills contain higher percentages of felsic intrusive and extrusive lithic fragments. Eastern Ross Sea till samples are compositionally similar to West Antarctic till, particularly in their abundance of quartz and dearth of mafic and extrusive lithic components. Central Ross Sea till exhibits compositional similarities to both East and West Antarctic source terranes including a mafic lithic component, and marks the confluence of ice draining from East and West Antarctica during the LGM, thus West Antarctic-derived ice streams did not advance into the western Ross Sea. This indicates that even if pre-LGM equivalents of the present Siple Coast ice streams existed, they did not simply expand allowing West Antarctic-derived ice to dominate the LGM Ross Ice Sheet.

1. Introduction

Ross Sea sediments across the continental shelf contain a long-term record of past fluctuations in the size and extent of the ice draining from East Antarctica and West Antarctica (Fig. 1). During the Last Glacial Maximum (LGM), both ice sheets advanced onto the continental shelf, contributing to the formation and expansion of the Ross Ice Sheet. Although the grounding line of LGM ice in the Ross Sea has been well constrained (e.g., Licht et al., 1996, 1999; Shipp et al., 1999), the relative contributions by East and West Antarctica remain uncertain. Constraining LGM ice flow paths provides important constraints for modeling the LGM paleoflow dynamics and reconstructing the style of Ross Ice Sheet retreat.

A conceptual model of the LGM Antarctic ice sheet in the Ross Embayment developed by Stuiver et al. (1981) assumes that the Siple Coast ice streams extended along seafloor troughs out to the continental shelf break and that most of the ice comprising the Ross Ice Sheet was supplied from West Antarctica (Fig. 2). Licht and Fastook (1998) reported a quasi-3D numerical simulation of ice advance and retreat for the Ross Ice Sheet that was constrained by marine geologic data, including maximum ice extent from the Ross Sea (Licht et al., 1996, 1999) (Fig. 2). The results of Licht and Fastook's (1998) model differ from Stuiver et al. (1981) and indicate that East Antarctic-derived ice dominates the western to central Ross Sea, and that the confluence with West Antarctic ice is in the central Ross Sea (CRS).

*Corresponding author. Tel.: 317 278 1343; fax: 317 274 7966.
E-mail address: klicht@iupui.edu (K.J. Licht).

0277-3791/$ - see front matter © 2005 Elsevier Ltd. All rights reserved.
doi:10.1016/j.quascirev.2004.10.017

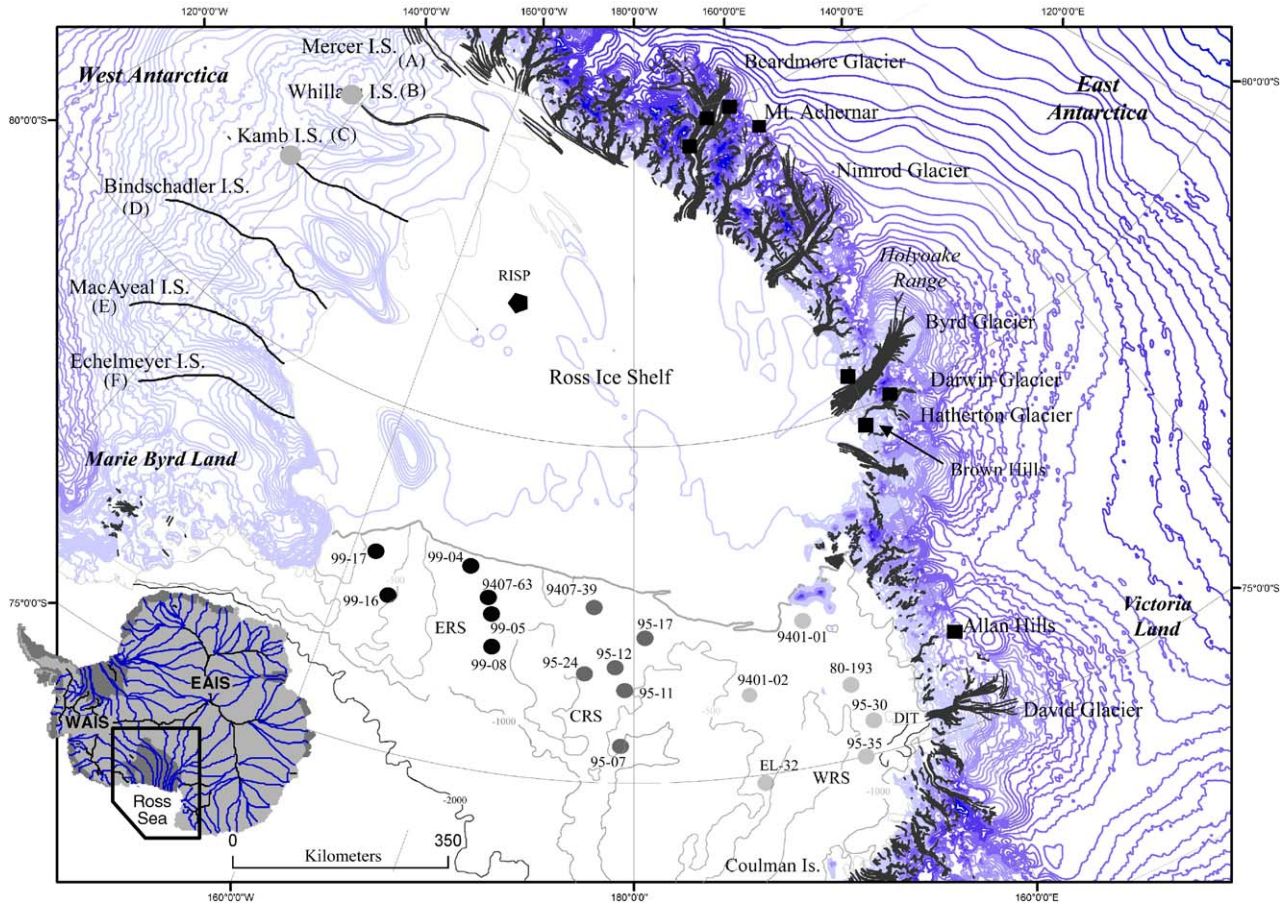

Fig. 1. Location map showing the Ross Embayment study area with approximate sampling locations and features pertinent to this study. Note that the Ross Sea has been divided into three areas; ERS, WRS, and CRS. Refer to Table 2 for the respective sample numbers at sampling locations. DIT = Drygalski Ice Tongue, RISP = Ross Ice Shelf Project core sites. Bathymetric contours are in meters. Inset map shows modern ice flow lines and the drainage basin for the Ross Sea (modified from Drewry, 1983). WAIS = West Antarctic ice sheet, EAIS = East Antarctic ice sheet.

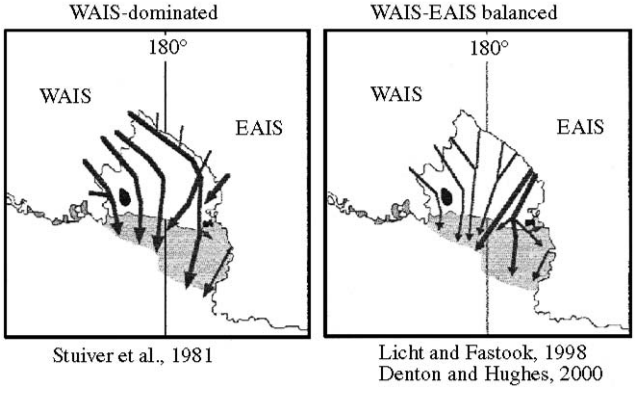

Fig. 2. Simplified schematic reconstructions illustrating the basic differences between the paleoice-flow models proposed by Stuiver et al. (1981) vs. Licht and Fastook (1998) and Denton and Hughes (2000). Wider lines indicate higher velocity ice flow. The shaded area shows the Ross Sea continental shelf. WAIS = West Antarctic ice sheet, EAIS = East Antarctic ice sheet.

This thermomechanical model allowed for basal sliding, accounted for isostatic adjustments, and was based on a 20 km grid. A reconstruction by Denton and Hughes (2000) based on ice extent and ice elevation data shows flow lines similar to the Licht and Fastook (1998) model. These models provide testable hypotheses of the LGM flowlines in the Ross Ice Sheet.

Many studies (i.e., Hughes, 1977; Balshaw, 1980; Domack et al., 1999; Shipp et al., 1999) have proposed that the NE–SW trending troughs, which are distinctive features of Ross Sea floor bathymetry (Fig. 1), were formed by ice streams within the Ross Ice Sheet and/or constrained flow during the LGM advance of the Ross Ice Sheet. Several studies interpret the troughs as remnant features sculpted by enlarged West Antarctic ice streams within the Ross Ice Sheet (Hughes, 1973; Shipp et al., 1999). However, no direct evidence ties the troughs to enlarged West Antarctic ice streams.

This study correlates the coarse sand composition of LGM till from across the Ross Sea with till from source areas in East and West Antarctica in order to identify past ice flow paths. We expand upon the results of previous provenance studies (Balshaw, 1980; Anderson et al., 1992) by including till samples from the source terranes, which provide an essential link between till

deposits on the Ross Sea continental shelf with mapped or inferred bedrock types. Based on the observed correlations between East and West Antarctic till with Ross Sea LGM till, we assess the previous models of paleo ice-flow dynamics for the Ross Ice Sheet.

2. Physical setting

The Ross Sea embayment is bounded on the west and south by the Transantarctic Mountains of Victoria Land and on the east by Marie Byrd Land (Fig. 1). Currently, much of the Ross Sea is covered by the Ross Ice Shelf (Fig. 1). Seaward of the Ross Ice Shelf, the continental shelf has an average depth of ~500 m and displays a reverse gradient typical of regions weighed down by large ice caps (Anderson, 1999). Ross Sea floor bathymetry is characterized by several northeast/southwest-trending troughs and ridges that cross the Ross Sea continental shelf (Fig. 1).

West Antarctica is an archipelago of islands nearly entirely covered by the West Antarctic ice sheet, which is mostly grounded below sea level. Major rock exposures in the West Antarctic basin that feeds the Ross Embayment are generally confined to the Marie Byrd Land Volcanic Province. The Transantarctic Mountains have substantial rock outcrop exposures and represent the boundary between the East and West Antarctic ice sheets (Fig. 1). Because the till composition in East and West Antarctica primarily reflects the local geological materials, an understanding of the regional geology encompassing the Ross Embayment is essential for determining the provenance of till across the Ross Sea continental shelf.

2.1. Geology and structure

2.1.1. East Antarctica and the Transantarctic Mountains

The East Antarctic craton has been tectonically and structurally stable since the break up of Gondwanaland beginning in the Jurassic. Generally, rocks comprising East Antarctica are older than West Antarctic rocks (Fig. 3) and much of what is known about East Antarctic geology relies on rock outcrops around its perimeter. Bushnell and Craddock (1970) report detailed descriptions of the rock units in East Antarctica, a majority of which are exposed in the Transantarctic Mountains (see also Stump, 1995). The Transantarctic Mountains contain diverse rock units (Fig. 3) spanning the Precambrian through the Quaternary and are composed of seven major rock groups: (from oldest to youngest) the Nimrod, Beardmore, Byrd, Granite Harbour Intrusives, Beacon, Ferrar, and McMurdo Volcanics groups.

The Archean–Early Proterozoic Nimrod Group is a heterogeneous metamorphic complex containing banded quartzofeldspathic to mafic gneiss, schist, quartzite, marble, as well as intrusive granitic to gabbroic rock, calc-silicate gneiss, relict eclogite, and pods of ultramafic rocks (Goodge et al., 1993; Goodge and Fanning, 1999). Igneous rocks initially formed ~3000 my BP as indicated by U–Pb dating of successive zircon growth were metamorphosed at 2955, 1720, and 530 Ma (Goodge and Fanning, 1999; Goodge et al., 1993). Overlying the Nimrod Group are upper Precambrian Beardmore Group rocks containing pelitic schist, hornfels, and metagraywacke (Laird et al., 1971; Myrow et al., 2002; Goodge et al., 2002).

The Beardmore Group is overlain by the Cambrian Byrd Group, which contains sedimentary and metasedimentary rock formations (Bushnell and Craddock, 1970; Myrow et al., 2002). The lowest unit is Shackleton limestone (with some oolitic units) and marble, while upper units contain quartzite, marble, conglomerate, sandstone and shale. Several areas of the Transantarctic Mountains and Marie Byrd Land contain exposures of the Cambrian–Ordovician Granite Harbour Intrusive Series that include biotite–hornblende granodiorite, hornblende granite, and biotite–muscovite–microcline adamellite. Overlying the Byrd Group is the Devonian–middle Triassic Beacon Supergroup that includes a sequence of quartz sandstone and basal conglomerate, tillite, and glacial fluvial sediments as well as a succession of sandstone, shale, and coal, intruded by dolerite dikes and plugs (Barrett, 1991). The Beacon Supergroup is overlain by the Triassic–Jurassic Ferrar Group, composed of basalt, tuff, and volcanic conglomerate with tholeiitic dolerite and intruded by dolerite sills.

Above the Ferrar group is the upper Tertiary–Quaternary McMurdo Volcanic Group, an extensive volcanic complex comprising part of eastern Victoria Land and extending into the western Ross Sea (WRS) (Fig. 3). The volcanic group contains volcanic centers ranging from small scoria cones and flows to large active volcanoes (Kyle, 1990). A wide range of extrusive rock types are associated with the McMurdo Volcanic Group, including rhyolites and basalts (Kyle, 1990).

2.1.2. West Antarctica

West Antarctica is largely characterized by the ~3000 km-long West Antarctic rift system that has produced episodic West Antarctic crustal extension since the Late Mesozoic (Behrendt and Cooper, 1991; Wilson, 1992; Dalziel and Lawver, 2001). The alkaline basaltic volcanic rocks comprising the West Antarctic Rift System today are associated with episodic late Cretaceous–Cenozoic rifting, which is characterized by limited extension activated by downfaulting beneath the Ross Sea continental shelf, accelerated rift-shoulder uplift, and associated bimodal alkalic volcanism throughout the area (Le Masurier, 1990; Behrendt

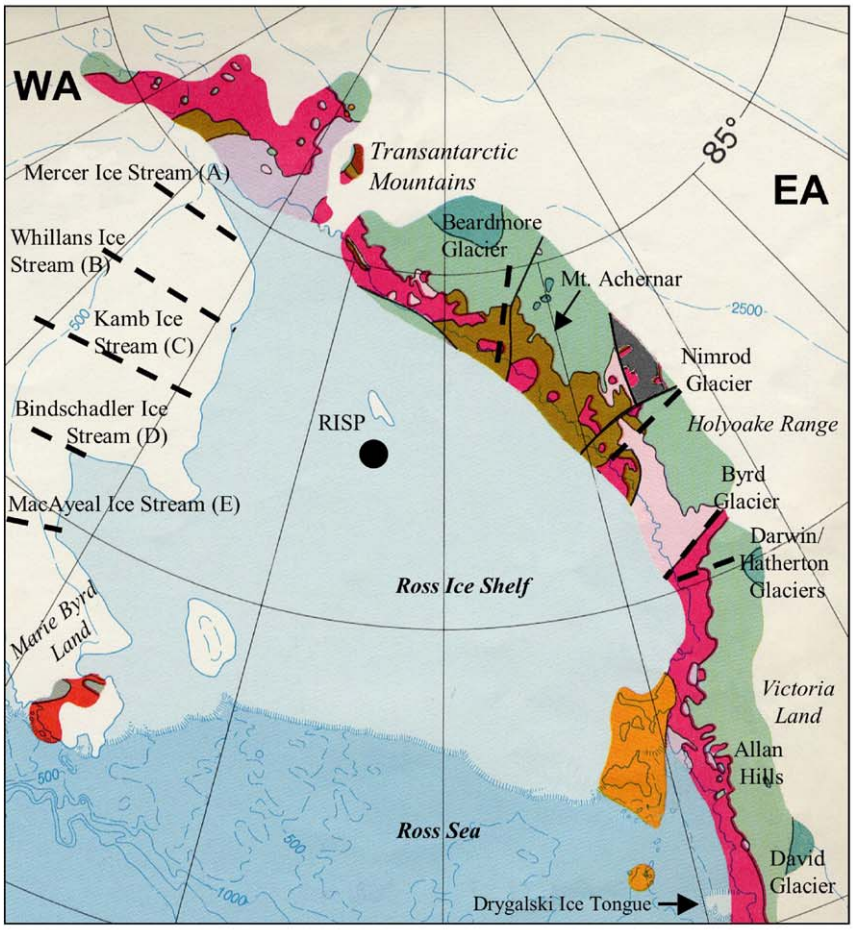

McMurdo Volcanic Group (olivine basalt, trachyte, kenyte, pyroclastic deposits) Upper Tertiary - Quaternary

Ferrar Group (tholeiitic flows, dolerite sills, agglomerate tuff, volcanic conglomerate) Triassic - Jurassic

Beacon Supergroup (conglomerate, sandstone, shale, tillite, glacial fluvial sediments, coal measures with tholeiitic dikes, sills, and plugs) Devonian – middle Triassic

Ford Granodiorite and Byrd Coast Granite (Paleozoic)

Granite Harbour Intrusives (biotite-hornblende granodiorite and hornblende granite) Cambrian - Ordovician

Byrd Group (marble, limestone, oolitic limestone, quartzite, conglomerate, sandstone, volcanic rocks, micaceous-microcline adamellite) Cambrian

Beardmore Group (pelitic schist, hornfels, metagraywacke, argillite) upper Precambrian

Nimrod Group (quartzite, marble, schist, diorite, gneiss, ecologite lenses) Precambrian

Basement Complex – metasedimentary rocks - Precambrian

Fig. 3. Generalized geologic map of the major bedrock groups in the Ross Embayment including the Transantarctic Mountains, Victoria Land, and western Marie Byrd Land. The dashed black lines show the approximate locations of glaciers and ice streams mentioned in the text. Modified from Bushnell and Craddock (1970).

et al., 1991; Lawver et al., 1991; Fitzgerald, 1992). This rift contains up to 600 m of basin-fill derived from erosion of the Transantarctic Mountains and marine deposition (Rooney et al., 1991; Scherer et al., 1998).

Because West Antarctica is largely covered by the West Antarctic ice sheet, rock exposures within the Ross Sea drainage basin are confined to nunatuks of Marie Byrd Land and the Transantarctic Mountains to the south (Fig. 3). The Marie Byrd Land Volcanic Province consists of north–south and east–west chains of Mesozoic–Cenozoic shield volcanoes, as well as areas where exposed Paleozoic basement rock has been

glacially sculpted into rectilinear nunatuks (Le Masurier and Rex, 1991). The shield volcanoes are composed of basaltic flows and tuff breccias and are overlain by felsic and intermediate flows and tuff breccias (Le Masurier and Rex, 1991). The late Paleozoic and Mesozoic basement rocks include the Ford Granodiorite and Byrd Coast Granite, as well as early Paleozoic argillites of the Swanson Formation (e.g., Le Masurier and Wade, 1976; Le Masurier and Rex, 1991; Luyendyk et al., 1991; Weaver et al., 1991). The exposed rock to the south of the West Antarctic rift within the Transantarctic Mountains is dominantly Granite Harbor Intrusive rocks with smaller amounts of Beardmore and Ferrar Group rocks (similar to Transantarctic Mountains rocks in East Antarctica).

Subglacial West Antarctic rocks within the rift are primarily interbedded volcanic and sedimentary strata, as revealed by magnetic and seismic studies (Jankowski and Drewry, 1981; Bentley, 1991). Behrendt et al. (1994) characterized the volcanic rocks as Cenozoic flood basalts that originated from a mantle plume (associated with rifting). However, overlying the basalt are Oligocene or younger terrigenous and glacial–marine sediment, which may be as thick as 600 m, the upper ~20 m of which corresponds to Plio–Pleistocene tills (Rooney et al., 1991; Tulaczyk et al., 1998). A large component of the rift sediments were likely transported from the slopes of the flanking Transantarctic Mountains and Marie Byrd Land Volcanic Province into the rift basin. Pelagic marine deposition likely took place during ice-free conditions in conjunction with terrigenous input, as evidenced by the presence of Miocene diatoms in the sediment (Scherer et al., 1998).

3. Till provenance studies in the Ross Embayment

The position of the maximum ice extent in the Ross Sea has been constrained by identifying the boundary between subglacial and glacial–marine sediment (Kellogg et al., 1979; Anderson et al., 1992; Licht et al., 1996, 1999; Domack et al., 1999), as well as the geometry of sedimentary packages and shelf morphologic features produced by glacial activity (e.g., Anderson et al., 1992; Shipp et al., 1999). LGM till thicknesses vary across the Ross Sea, with the thickest strata occurring in the ERS, CRS, and on the outer shelf (Shipp et al., 1999). WRS LGM sediments exhibit variable thickness, with LGM till generally confined to areas south of Coulman Island (Licht et al., 1996, 1999; Domack et al., 1999; Shipp et al., 1999). The position of maximum grounded ice extent in the ERS and CRS approximately follows the profile of the continental shelf break (Anderson, 1999; Shipp et al., 1999; Licht and Andrews, 2002). Maximum ice extent in the WRS, which is well short of the shelf break indicates that the Ross Ice sheet did not reach an equilibrium position during the LGM (Licht, 2004).

Seismic surveys and sediment studies have aided in determining an accurate understanding of the extent of grounded ice across the Ross Sea continental shelf. Anderson et al. (1992) and Shipp et al. (1999) interpreted seismic profiles from the Ross Sea to delineate the position of the Ross Ice Sheet grounding line. Based on the position of glacial features and sediment thicknesses from seismic surveys, Shipp et al. (1999) identified the maximum grounding line at the shelf break in the CRS and ERS and slightly seaward of Coulman Island in the WRS (Fig. 1), consistent with the earlier results of sediment analysis from WRS cores (Licht et al., 1996, 1999).

Licht et al. (1999) differentiated subglacial and glacial marine lithofacies in WRS sediments using particle size, total organic carbon (TOC), carbonate content, and tephra layers in order to determine the maximum extent of grounded ice. Licht et al. (1996, 1999) identified the WRS grounding line just south of Coulman Island based on the distribution of glacial till in piston cores; a slightly more extensive ice sheet was described by Domack et al. (1999) following the collection of additional cores. Lithologic data from marine sedimentary cores and AMS radiocarbon dates indicate that LGM ice reached its maximum position in the CRS by about 13,800 ^{14}C yr BP (Licht and Andrews, 2002) and ice retreated back to Ross Island by ~7000 ^{14}C yr BP (Licht et al., 1996; Hall and Denton, 1999). Although the maximum ice extent in the Ross Sea has been mapped, the expansion style of the ice sheet remains uncertain.

Two studies have focused on characterizing Ross Sea sediment composition, with the aim of determining Ross Sea till provenance. Balshaw (1980) examined the clay mineralogy of Ross Sea till and found that the highest concentrations of smectite occur in the ERS troughs with lower concentrations of smectite in the WRS and CRS troughs. Based on the Hughes (1977) flow lines, which show an expanded West Antarctic ice sheet that followed Ross Sea bathymetry, Balshaw (1980) speculated that low smectite concentrations in the WRS were derived from ice streams A–C and high smectite concentrations in the CRS and ERS were derived from ice streams D–F. Anderson et al. (1992) observed significant east-to-west variability in the pebble, coarse sand, and heavy mineral composition of Ross Sea till. They found that the WRS sand fraction is dominantly composed of rounded quartz, granite, diamicton fragments, volcanic glass, and minor diabase and litharenite. The ERS sand fraction is quite different from the WRS till and is composed of schist and smaller quantities of gneiss, rounded quartz and granite. East-CRS sediments have a composition similar to ERS sediments, whereas west-CRS sediments have a composition similar to WRS

sediments. Anderson et al. (1992) linked the pebble-sized fraction from WRS till to the Beacon Supergroup, Ferrar Group, McMurdo Volcanic Group and exposures of biotite schists and gneisses near Priestly Glacier. The previous studies by Balshaw (1980) and Anderson et al. (1992) provide valuable information about Ross Sea till composition, however, the lack of till samples from the East and West Antarctic sources areas limits their ability to provide a robust provenance-based reconstruction of past ice-flow paths.

In order to better understand Antarctica's Cenozoic glacial history and the erosion history of the Transantarctic Mountains, sand provenance studies of glacial deposits contained in the MSSTS-1 and CIROS-1 cores collected in McMurdo Sound, were completed on the 62–500 μm using the Gazzi–Dickinson method (Barrett et al., 1986; George, 1989). Because these cores were collected close to shore, they clearly reflect the local geological source terranes, including the crystalline basement, Beacon Supergroup, Ferrar Group and McMurdo Volcanic Group. Both cores show substantial changes in sand composition throughout the Cenozoic and help constrain the timing of major erosion of the Beacon Supergroup, as well as the development of local volcanism. The more recently collected cores from the Cape Roberts Project recovered thicker Quaternary sections approximately 40 km north of the CIROS and MSSTS core sites. The Cape Roberts Project cores were collected <20 km offshore and are also dominated by rock and mineral fragments from the Beacon Supergroup, Ferrar Group and McMurdo Volcanic Group (e.g., Cape Roberts Science Team, 1998, Smellie et al., 2001).

Tulaczyk et al. (1998) examined till retrieved from beneath the Whillans (B) and Kamb (C) Ice Streams. Coring recovered an extremely poorly sorted diamicton with sparse pebbles. The sand fraction averages $59\pm5\%$ quartz, $27\pm3.5\%$ feldspar, and $16\pm3.5\%$ lithic fragments. Until now, no studies have analyzed and compared Ross Sea tills with representative till samples from the plausible East and West Antarctic source areas.

4. Methods

The sand fraction of Late Quaternary till samples from several East Antarctic outlet glaciers in the Transantarctic Mountains, the Whillans Ice Stream (B), Kamb Ice Stream (C), and samples from cores across the Ross Sea (Fig. 1 and Table 1) were analyzed and compared. All of these till samples were collected during previous cruises and field seasons by various investigators (Table 1). East Antarctic till samples were available from near four glaciers; Byrd Glacier, Darwin Glacier, Hatherton Glacier and Beardmore Glacier, as well as from Mt. Achernar and the Allan Hills (Fig. 1). Due to their relative inaccessibility, fewer West Antarctic samples were available for analysis than East Antarctic samples. The West Antarctic till samples were retrieved at two sites from beneath the Whillans and Kamb Ice Streams.

A total of 20 piston cores collected during the Ross Ice Shelf Project (RISP) and six cruises: Nathaniel B. Palmer, 94–01, −07, 95–01, 99–02, Eltanin 32, and Deep Freeze 80 (Table 1) were subsampled for analysis. Subsamples were chosen from cores retrieved landward of the LGM grounding line in the Ross Sea. The sites in the CRS and ERS are associated with mega-scale glacial lineations and drumlins, whereas these features are not as common near the WRS sample sites (Shipp et al., 1999; Anderson et al., 2002). Because of the limitations of piston coring in deep water, it is not possible to determine the precise location of each core with respect to the subglacial bedforms. In several CRS cores sampled for this study (NBP9501-07, 12, 17 and 24), Licht (1999) described strong vertical fabric in all size fractions of the till, suggesting major subglacial deformation in this region. These vertical fabrics are absent or rare in other regions of the Ross Sea.

Although the gravel fraction of till can provide valuable provenance information, it was not included in this study because the core samples did not contain enough gravel to provide statistically meaningful results. Andrews (2000) argued that the sand fraction makes up a relatively small fraction of glacial sediments. However, the till samples analyzed in this study average 33% sand content and therefore represent an important fraction of the till. As a complement to this study, Farmer et al. (2004) performed isotopic analyses on the <63 μm fraction of a similar sample suite.

4.1. Thin section preparation and point counting

A representative subsample of the 500–2000 μm sand fraction from ~3 g of each of the 47 till samples was analyzed petrographically. The petrography of sand fraction <500 μm proved to be exceedingly difficult to characterize accurately with the Indiana point-counting method, and was therefore excluded. Sand samples were impregnated with blue dye resin and made into thin sections following standard thin section preparation procedures, taking care to place as many grains as possible in the plane of the section.

The Indiana point counting method (Suttner, 1974; Suttner et al., 1981) characterizes individual minerals and rock fragments (a rock-fragment consists of two or more minerals or mineral phases) and was chosen over the Gazzi–Dickinson Method (Gazzi, 1966; Dickinson, 1970) because it accounts for both lithology and mineralogy. By categorizing lithic fragments and

Table 1
Latitude, longitude, sampling information for Ross Sea and RISP cores, as well as moraine samples from West and East

Core ID	Latitude	Longitude	Sampling depths (cm)	Water depth (m)
Ross Sea[a]				
DF80-193	−76.550	165.017	49–51, 99–101, 149–150, 150–152	732
EL32-13	−74.96	172.157	50, 100, 151	537
RISP 78-8	−82.220	−168.39	42–44	587
RISP 78-14	−82.220	−168.38	99–91	587
NBP9401-01	−77.194	167.888	104, 151	939
NBP9401-02	−76.28	169.704	150–152	679
NBP9407-39	−77.92	−178.000	100–102	694
NBP9407-63	−77.33	−169.181	112–114	582
NBP9501-07	−75.625	−178.587	13–28	449
NBP9501-11	−76.45	−179.087	48–50, 100–102	659
NBP9501-12	−76.785	−177.882	56–65	568
NBP9501-17	−77.452	179.050	49, 48–50,100–102,155–171	732
NBP9501-24	−76.607	−175.417	74–90	585
NBP9501-30	−76.06	164.585	47–49, 123–125	752
NBP9501-35	−75.17	164.493	49–51, 99–101	1256
NBP9902-04	−78.15	−168.580	10–12, 97–99	618
NBP9902-05	−77.25	−169.386	105–107	603
NBP9902-08	−76.87	−170.015	103–105	540
NBP9902-16	−77	−163.385	102–104	656
NBP9902-17	−77.72	−161.862	104–106	715
Source areas[b]				
UpD 98-4-1-1[c]	−81.441	−140.033	0–10	N/A
UpC 00-4-1-1	−82.259	−136.241	0–10, 50	N/A
UpB ISB89-4	−83.29	−138.12	0–10, 50	N/A
Hatherton/Darwin	−80	160	48–83	N/A
Darwin/Brown Hills	−79.8	158.5	0–18	N/A
Darwin Terminus	−84.8	160	2–60	N/A
Hatherton (Derrick Peak)	−80.1	156.3	21–200	N/A
upper Beardmore	−85.1	163.1	60–80	N/A
upper Beardmore	−85.8	158.1	23–65	N/A
central Beardmore	−84.3	169.7	8–45	N/A
lower Byrd Glacier	−80.5	160.0	0.5–20	N/A
Mt Achernar	−84.2	160.9	Surface	N/A
Allan Hills	−76.7	159.5	Surface	N/A

[a]Sediment subsamples were provided by the Antarctic Research Facility at Florida State University and the Institute of Arctic and Alpine Research at the University of Colorado, Boulder.
[b]Samples provided by G. Faure, J Bockheim, H. Engelhardt. East Antarctic latitudes and longitudes are approximations based on reported sampling locations.
[c]UpD (Bindschadler) Ice Stream sample was too small for sand provenance analysis and therefore is not included in Tables 3 and 4. Particle size results for this sample are reported in Fig. 9.

individual mineral grains, more categories become available, allowing for a more detailed description of each till sample (Table 2).

With the goal of making at least 300 counts for each sample, systematic transects were carefully made across each thin section counting every grain. It was not always possible to count 300 grains per thin section because of the small size of the same samples (Table 3). Samples SAL 1, 106, 122, 123, 186, 193, and 194 were point counted twice to test reproducibility and the replicates were averaged for the analysis (Table 3). The point counts were reproducible with differences typically on the order of 1–4%. Largest errors (up to 14%) occurred in the quartz point counts among West Antarctic samples where it was occasionally difficult to differentiate between quartz grains with wavy extinction and quartzite lithic fragments. These errors have little effect on determining the till provenance because quartz was not a clear discriminating factor between samples from the source terranes and Ross Sea regions.

4.2. Particle size analysis

Particle size analyses were completed for all samples in order to explore the potential relationship between particle size distributions and sand composition. Approximately 2 g of material was separated from the bulk

Table 2
Lithic fragment classification used for point counts

Category	Classification criteria
Sedimentary lithic fragments	
Silt/sandstone	Distinct sand and/or silt size grains ± finer matrix material
Mudstone	Contain silt- and clay-sized particles difficult to determine exact composition
Claystone	No discernable grain boundaries
Intrusive igneous fragments	Large crystals with interlocking boundaries
Felsic	Quartz + K-spar ± plagioclase, biotite, hornblende, muscovite
Intermediate	± quartz + > 50% plagioclase + minor K-spar ± hornblende, biotite, clinopyroxene
Mafic	> 50% plagioclase + ortho/clinopyroxene, ± olivine, iron oxide
Extrusive igneous fragments	± Large crystals with matrix of smaller elongate angular crystals
Basalt ± andesite ± rhyolite	Fine-grained matrix ± zoned and/or polysynthetic twinned plagioclase ± volcanic glass ± abundant opaque minerals ± clinopyroxene
Metamorphic fragments	
Quartzite	Intergrowth of quartz crystals
Marble	Twinned calcite
Schist	Grains exhibit fabric

till samples for particle size analysis. Samples were sieved to obtain the $<2000\,\mu m$ fraction, and treated with 35% H_2O_2 to remove organic material, and stored in sodium metaphosphate. Each sample was analyzed 3–5 times in a Malvern Mastersizer 2000 laser particle size analyzer and the size distribution as well as the average particle size value is reported for each sample (Fig. 9 and Table 3).

4.3. Statistical methodology

Cluster analysis was performed on point count data (Sneath, 1977), excluding minerals present in concentrations <5% and quartz, which has high concentrations in nearly all samples. Removing minerals that are not abundant (e.g., muscovite) or ubiquitous (e.g., quartz) reduced noise within the cluster analysis. The results of Euclidean Distance Average Linkage Method of cluster analysis were used to create a dendrogram where samples exhibiting the strongest compositional similarities are clustered (Davis, 1986). The shorter the average Euclidean distance linking two samples, the greater the similarity between the samples. The significance of the groups determined by cluster analysis was tested using discriminant analysis (Systat, 1998). Weighted combinations of all the original point count percentage data were used to form variables called discriminant functions. The weighting of each variable indicates their importance in forming the groups delineated by cluster analysis. Plots of centroids (average locations) for each group in discriminant function space, and their 95% confidence intervals illustrate the significance of a group. All statistical analyses were completed with Systat Version 8.0 for PC (Systat, 1998).

5. Results

5.1. East Antarctica

Table 3 shows the results of the coarse sand fraction point counts for all the till samples including ten samples from six different locations along the Transantarctic Mountains. On average, the East Antarctic samples contain approximately equal numbers of lithic fragments and individual mineral grains. In decreasing concentrations, East Antarctic samples contain quartz (33.1 ± 20.2%), sedimentary lithic fragments (21.1 ± 28.2%), mafic intrusive lithic fragments (15.6 ± 14.6%), and metamorphic lithic fragments (7.5 ± 8.3%) (Fig. 5, Table 3). The metamorphic fragments are typically quartzite with minor foliated lithic fragments. Sample SAL 194 from lower Byrd Glacier is the only East Antarctic sample with quartz <20% and that contains large concentrations of calcite (70.1%) and marble fragments (12.2%).

Spatial variability in the petrologic composition exists between samples, reflecting the diverse bedrock sources within the Transantarctic Mountains and East Antarctica. The proportions of calcite, sedimentary lithic fragments (mudstone), mafic intrusive lithic fragments, metamorphic lithic fragments, and plagioclase exhibit the largest spatial variability, as is evident by the large standard deviations from the mean values for all East Antarctic samples for these variables (Table 3).

5.2. West Antarctica

Four samples were analyzed from cores taken beneath the Whillans Ice Stream (B) and Kamb Ice Stream (C) (Fig. 1). In order of decreasing abundance, they contain

Table 3
Percenatage data from point counts made on each grain mount from the source terranes, RISP and the Ross Sea

Location	Depth (cm)	Sample ID	Qtz	Pyrox	K-spar	Plag	Cal	Olv	Iron ore	Musc	Biot	Chlor	Opq	Other/ unk	Silt/ s.s.	Mudst	Clayst	L.s.	Extr	Maf	Int	Fel	Meta	*n*	*d* (μm)
East Antarctic samples																									
Hatherton/Darwin (78-14)	48–83	SAL 106	67.2	3.9	0.3	3.2	0.0	0.0	0.0	0.0	0.0	0.0	0.0	0.9	1.9	1.6	0.6	0.0	0.3	17.5	0.3	0.6	2.3	308	203.04
		SAL 106 replicate	67.0	3.8	0.0	4.5	0.0	0.0	0.0	0.0	0.0	0.0	0.0	0.0	0.6	0.3	0.0	0.0	0.0	21.3	1.3	0.6	0.3	310	—
		SAL 106 mean	67.1	3.9	0.2	3.9	0.0	0.0	0.0	0.0	0.0	0.0	0.0	0.5	1.3	1.0	0.3	0.0	0.2	19.4	0.8	0.6	1.3		
Darwin/Brown Hills (78-71)	0–18	SAL 192	21.2	0.0	1.0	24.6	0.0	0.0	0.0	1.0	1.3	0.0	1.0	0.6	0.0	38.4	1.0	0.0	0.3	0.3	0.0	8.8	0.3	297	128.67
Darwin Terminus (78-62)	2–60	SAL 114	27.6	7.0	0.0	0.4	0.4	0.0	0.0	0.0	0.0	0.0	0.0	1.5	4.8	5.9	4.8	0.0	0.0	47.8	0.0	0.0	2.9	272	4.44
Hatherton (78-55)	21–100	SAL 187	36.9	4.0	0.0	0.0	0.0	1.4	0.0	0.0	0.0	0.0	0.0	0.0	6.1	0.0	0.0	0.0	0.0	23.0	0.0	6.1	26.4	304	375.82
Lower Byrd (78-66)	0.5–20	SAL 194	5.5	0.3	0.3	0.3	70.0	0.3	0.3	0.0	0.0	0.0	0.0	0.3	0.0	0.0	0.0	0.0	0.0	12.0	0.3	0.3	13.0	294	
		SAL 194 replicate	5.6	0.0	0.0	0.0	70.1	0.0	0.0	0.0	0.0	0.0	0.0	0.0	1.0	0.0	0.0	0.0	0.0	12.0	0.0	0.0	11.3	301	—
		SAL 194 mean	5.6	0.2	0.2	0.2	70.1	0.2	0.2	0.0	0.0	0.0	0.0	0.2	0.5	0.0	0.0	0.0	0.0	12.0	0.2	0.2	12.2		
Central Beardmore (85-44)	8–45	SAL 193	67.6	0.8	1.2	0.4	0.0	0.0	0.4	0.0	0.0	0.0	0.0	0.0	14.7	0.0	1.2	0.0	0.0	0.0	2.7	0.0	11.1	252	49.09
		SAL 193 (replicate)	65.1	0.4	0.7	0.4	0.4	0.0	0.0	0.0	0.0	0.0	0.0	0.0	12.1	2.5	1.8	0.0	0.0	0.0	3.9	0.7	12.1	281	—
		SAL 193 mean	66.4	0.6	1.0	0.4	0.2	0.0	0.2	0.0	0.0	0.0	0.0	0.0	13.4	1.3	1.5	0.0	0.0	0.0	3.3	0.4	11.6		
Upper Beardmore (85-34)	60–80	SAL 119	42.7	1.1	0.0	1.7	0.0	0.0	0.0	0.0	0.0	0.0	1.1	0.4	9.6	21.3	8.4	0.0	1.7	10.0	0.0	0.0	0.0	239	80.15
Upper Beardmore (85-17)	23–65	SAL 186	32.0	14.0	0.4	0.9	0.0	0.0	0.0	0.0	0.0	0.0	0.0	0.0	6.0	0.0	0.4	0.0	0.0	33.0	0.9	0.0	12.0	338	251.17
		SAL 186 replicate	32.2	14.0	0.4	0.9	0.0	0.0	0.0	0.0	0.0	0.0	0.0	0.0	6.0	0.0	1.0	0.0	0.0	33.0	1.0	0.0	12.0	208	
		SAL 186 mean	32.1	14.0	0.4	0.9	0.0	0.0	0.0	0.0	0.0	0.0	0.0	0.0	6.0	0.0	0.7	0.0	0.0	33.0	1.0	0.0	12.0		
Mt. Achernar (Faure)	Surface	SAL 226	27.0	0.3	0.0	0.9	0.3	0.0	0.0	0.0	0.0	0.0	2.7	0.0	0.0	52.5	4.5	0.0	0.9	2.7	0.0	3.3	0.0	337	5.67
Allan Hills (Faure)	Surface	SAL 227	31.9	1.7	0.2	0.0	0.2	0.0	0.0	0.0	0.0	0.0	0.2	0.0	0.0	46.4	2.0	0.0	0.7	11.2	1.0	1.0	3.2	401	23.50
		East Antarctic mean	33.1	3.0	0.3	3.0	12.8	0.2	0.1	0.1	0.1	0.0	0.5	0.3	3.8	15.2	2.1	0.0	0.3	15.6	0.6	1.9	7.5		103.04
		East Antarctic SD	20.2	4.3	0.4	7.2	28.3	0.4	0.1	0.3	0.4	0.0	0.9	0.5	4.6	20.9	2.7	0.0	0.5	14.6	1.0	3.0	8.3		142.21
West Antarctic samples																									
Whillans Ice Stream	0–10	SAL 1 (UpB 89-4)	68.2	0.1	2.1	5.9	0.0	0.0	0.0	0.0	0.0	0.0	0.0	0.1	0.1	1.5	0.0	0.0	0.0	0.0	0.0	13.6	7.6	236	22.52
		SAL 1 replicate	48.7	0.4	1.1	3.3	0.0	0.0	0.4	0.0	0.0	0.0	0.0	0.0	0.2	12.0	2.9	0.0	0.0	0.7	5.1	8.0	17.1	275	—
		SAL 1 mean	58.5	0.3	1.6	4.6	0.0	0.0	0.2	0.0	0.0	0.0	0.0	0.1	0.2	6.8	1.5	0.0	0.0	0.4	2.6	10.8	12.4		
Whillans Ice Stream	95–100	SAL 3 (UpB 89-4)	73.8	0.5	1.0	5.1	0.0	0.0	0.5	0.0	0.0	0.0	0.0	0.5	1.2	3.1	1.2	0.0	0.5	0.0	0.5	12.3	5.1	162	45.72
Kamb Ice Stream	Surface	SAL 122 (00-4-1-1)	53.0	0.4	4.1	5.8	0.0	0.0	0.0	0.0	0.4	0.0	0.8	2.5	13.2	0.4	3.0	0.0	7.3	0.0	0.4	7.4	11.5	262	152.14
		SAL 122 replicate	51.2	0.0	3.2	8.7	0.0	0.0	0.0	0.0	0.0	0.0	1.5	0.0	10.2	0.0	0.0	0.0	3.6	0.0	0.0	11.7	9.0	205	—
		SAL 122 mean	52.1	0.2	3.7	7.3	0.0	0.0	0.0	0.0	0.2	0.0	1.2	1.3	11.7	0.2	1.5	0.0	5.5	0.0	0.2	9.6	10.3		
Kamb Ice Stream	95–100	SAL 123 (00-4-1-1)	43.5	0.0	0.5	25.2	0.0	0.0	0.0	0.0	0.0	0.0	1.5	0.0	2.3	3.8	3.1	0.0	0.0	0.0	0.0	18.3	0.0	107	37.02
		SAL 123 replicate	55.0	0.0	2.0	20.0	0.0	0.0	0.0	0.0	0.0	0.0	3.0	0.0	0.0	0.0	3.0	0.0	1.0	0.0	0.0	16.0	0.0	100	—
		SAL 123 mean	49.3	0.0	1.3	22.6	0.0	0.0	0.0	0.0	0.0	0.0	2.3	0.0	1.2	1.9	3.1	0.0	0.5	0.0	0.0	17.2	0.0		
		West Antarctic mean	58.4	0.2	1.9	9.9	0.0	0.0	0.2	0.0	0.1	0.0	0.9	0.5	3.6	3.0	1.8	0.0	1.6	0.1	0.8	12.5	6.9		45.72
		West Antarctic SD	11.0	0.2	1.2	8.6	0.0	0.0	0.2	0.0	0.1	0.0	1.1	0.6	5.5	2.8	0.8	0.0	2.6	0.2	1.2	3.3	5.5		59.31
RISP samples																									
RISP (78-8)	42–44	SAL 219	45.9	0.0	0.0	0.5	3.8	0.0	0.0	0.5	0.0	0.0	0.0	0.0	0.5	13.7	6.0	0.0	8.2	0.5	0.0	19.1	1.1	183	6.70
RISP (78-44)	99–101	SAL 222	57.9	0.0	0.7	1.4	0.0	0.0	0.0	0.7	0.0	0.0	0.0	0.0	0.0	10.7	10.7	0.0	1.4	0.0	0.0	13.6	2.9	140	14.76
		RISP mean	51.9	0.0	0.4	1.0	1.9	0.0	0.0	0.6	0.0	0.0	0.0	0.0	0.3	12.2	8.4	0.0	4.8	0.3	0.0	16.4	2.0		10.73
Western Ross Sea samples																									
DF80-193	49–51	SAL 376	40.6	3.5	0.0	5.9	0.0	0.4	0.8	0.0	0.0	0.0	1.6	0.8	0.0	16.9	1.6	0.0	3.9	9.8	0.0	10.6	3.6	254	5.41
DF80-193	99–101	SAL 373	40.5	2.4	0.0	4.8	0.0	0.0	0.0	0.0	0.0	0.0	1.2	2.4	0.0	28.6	0.0	0.0	8.3	8.3	0.0	3.6	0.0	84	5.91
DF80-193	149–151	SAL 403	66.0	2.4	0.0	4.4	0.0	0.0	0.0	0.0	0.0	0.0	0.5	2.0	0.0	17.4	3.5	0.0	7.3	7.3	0.0	3.9	0.5	206	8.99
EL32-13	49–51	SAL 406	32.8	2.6	0.4	3.7	0.0	0.0	0.0	0.0	0.0	0.0	2.9	1.5	0.0	14.9	5.2	0.0	15.7	11.9	0.0	6.7	1.4	268	9.43
EL32-13	100–102	SAL 407	40.1	3.3	2.8	2.8	0.0	0.5	0.0	0.0	0.5	0.0	3.3	2.3	1.4	11.3	5.2	0.0	5.7	8.0	0.0	10.8	0.9	212	10.43
EL32-13	149–151	SAL 408	43.8	0.0	0.8	6.6	0.0	0.0	0.0	0.0	0.0	0.0	1.7	3.4	0.0	8.3	3.3	0.0	9.0	9.0	0.0	14.0	0.0	121	9.74

Table 3 (*continued*)

Location	Depth (cm)	Sample ID	Qtz	Pyrox	K-spar	Plag	Cal	Olv	Iron ore	Musc	Biot	Chlor	Opq	Other/ unk	Silt/ s.s.	Mudst	Clayst	L.s.	Extr	Maf	Int	Fel	Meta	*n*	*d* (μm)
NBP9401-01	103–105	SAL 371	33.3	5.8	1.1	8.0	0.0	0.0	0.0	0.0	0.0	0.0	2.2	2.2	0.4	27.0	27.2	0.0	4.3	3.6	0.0	5.1	1.5	276	9.04
NBP9401-01	150–152	SAL 371	29.6	1.1	0.7	1.8	0.0	0.4	1.5	0.0	0.0	0.4	1.5	0.8	0.0	39.8	11.7	0.0	2.6	4.0	0.0	2.9	1.5	274	9.42
NBP9401-02	150–152	SAL 374	36.7	3.3	1.3	7.3	0.0	2.7	0.0	0.0	0.0	0.0	5.3	0.7	0.0	5.3	0.4	0.0	15.3	9.0	0.0	10.0	1.3	150	6.75
NBP9501-35	49–51	SAL 368	63.8	3.7	0.0	4.8	0.0	0.3	0.3	0.0	0.0	0.0	0.3	0.6	1.1	2.2	3.4	0.0	0.8	11.2	0.0	7.6	0.3	356	185.63
NBP9501-35	99–101	SAL 369	52.6	1.9	2.5	4.9	0.2	0.8	0.2	0.0	0.0	0.0	0.2	0.2	1.2	4.5	1.9	0.0	1.6	17.1	0.0	7.2	3.1	485	103.34
NBP9501-30	47–49	SAL 405	54.0	4.8	0.5	4.8	0.0	0.3	0.0	0.0	0.3	0.3	0.8	1.1	0.8	4.2	0.5	0.0	3.4	14.8	0.3	8.5	0.8	378	13.53
NBP9501-30	123–125	SAL 404	55.4	3.3	0.3	8.5	0.0	0.0	0.0	0.3	0.0	0.0	0.3	0.0	0.0	6.2	2.3	0.0	0.3	11.1	0.0	8.8	3.2	307	51.46
		WRS mean	45.3	2.9	0.8	5.3	0.0	0.4	0.2	0.0	0.1	0.1	1.7	1.4	0.4	14.4	5.1	0.0	6.0	9.6	0.0	7.7	1.4		33.01
		WRS SD	11.9	1.5	0.9	2.0	0.1	0.7	0.4	0.1	0.2	0.1	1.5	1.0	0.5	11.4	7.3	0.0	5.0	3.8	0.1	3.3	1.2		53.59
Eastern Ross Sea samples																									
NBP9407-63	112–114	SAL 142	75.3	0.0	1.3	3.9	1.3	0.0	0.0	0.0	0.4	0.0	0.9	3.0	0.0	0.9	3.0	0.0	2.6	0.0	0.0	7.4	0.0	231	11.86
NBP9902-04	10–12	SAL 138	69.0	0.0	1.2	1.2	0.0	0.0	0.6	0.0	0.0	0.0	0.6	5.4	0.0	3.0	3.7	0.0	3.7	0.0	0.6	10.4	0.0	164	21.33
NBP9902-04	97–99	SAL 169	64.1	0.5	2.0	1.5	1.0	0.0	0.0	0.5	0.0	0.0	1.5	3.5	0.0	4.6	7.2	0.0	1.5	0.0	0.0	9.7	2.0	195	20.84
NBP9902-05	105–107	SAL 177	78.8	0.0	5.6	7.1	0.0	0.0	0.0	0.0	0.6	0.0	0.6	0.0	0.3	0.6	0.0	0.0	0.0	0.0	0.0	6.2	0.3	354	9.34
NBP9902-08	103–105	SAL 178	65.6	0.0	1.6	3.6	0.0	0.0	0.0	0.3	0.0	0.0	0.3	1.0	1.0	3.3	2.6	0.0	0.7	0.0	0.0	16.0	3.9	305	—
NBP9902-16	102–105	SAL 306	84.8	0.0	0.6	1.8	0.0	0.0	0.0	0.3	0.0	0.0	0.6	1.2	0.0	0.9	3.0	0.0	0.3	0.0	0.0	5.7	0.3	336	16.84
NBP9902-17	104–106	SAL 141	76.0	0.0	0.5	0.0	0.5	0.0	0.0	0.0	0.0	0.0	0.5	0.5	2.0	6.6	5.6	0.0	0.0	0.0	0.0	6.1	1.5	196	8.31
		ERS mean	73.4	0.1	1.8	2.7	0.4	0.0	0.1	0.2	0.1	0.0	0.7	2.1	0.5	2.8	3.6	0.0	1.3	0.0	0.1	8.8	1.1		14.76
		ERS SD	7.5	0.2	1.7	2.4	0.6	0.0	0.2	0.2	0.3	0.0	0.4	1.9	0.8	2.2	2.3	0.0	1.4	0.0	0.2	3.7	1.4		5.72
Central Ross Sea samples																									
NBP9501-7	13–28	1.5 (95-7)	33.7	2.2	0.0	10.1	1.1	0.0	0.0	0.0	0.0	0.0	0.0	0.0	0.0	14.6	4.5	0.0	1.1	1.1	2.4	20.2	7.8	89	5.15 (@19 cm)
NBP9501-12	56–65	2.3 (95-12)	35.8	0.0	2.1	9.5	0.0	0.0	0.0	0.0	1.1	0.0	1.1	0.0	0.0	17.9	5.3	0.0	2.1	1.1	3.2	18.9	2.1	95	5.61 (@ 65 cm)
NBP9501-24	74–90	3.3 (95-24)	46.0	0.0	2.0	4.0	0.0	0.0	0.0	0.0	0.0	0.0	0.0	0.0	0.0	18.0	4.0	0.0	2.0	2.0	2.0	16.0	4.0	50	5.61 (@ 131 cm)
NBP9407-39	100–102	SAL 283	5.5	0.0	0.0	0.0	0.0	0.0	0.0	0.0	0.0	0.0	0.0	0.0	0.0	88.6	4.0	0.0	0.5	0.0	0.0	1.0	0.5	201	5.13
NBP9501-11	48–50	SAL 537	56.8	1.5	2.0	3.0	0.5	0.0	0.0	0.0	0.2	0.2	0.7	0.5	0.2	15.2	2.0	0.7	1.2	2.2	0.7	10.1	1.2	405	9.41
NBP9501-11	100–102	SAL 538	44.4	6.1	1.9	3.5	0.8	0.0	0.0	0.3	0.0	0.0	0.5	0.5	1.0	27.0	0.5	0.5	1.3	4.3	0.3	4.8	3.0	374	8.78
NBP9501-17	48–50	SAL 540	49.3	1.6	1.6	2.7	0.0	0.0	0.0	0.0	0.3	0.3	0.5	0.3	0.2	20.8	3.7	0.3	0.5	1.1	1.3	12.0	2.7	375	29.73
NBP9501-17	49	SAL 230	47.9	0.0	1.4	5.0	0.7	0.0	0.0	0.0	0.0	0.0	0.0	0.0	0.0	36.4	1.4	0.0	0.0	0.0	2.1	4.3	0.7	140	—
NBP9501-17	100–102	SAL 543	49.7	1.9	1.9	1.9	0.6	0.0	0.0	0.6	0.6	0.0	0.6	0.3	0.3	20.4	1.2	2.8	0.0	2.5	1.2	9.9	3.7	324	14.13
NBP9501-17	153–155	SAL 534	44.1	4.1	1.6	3.4	2.8	0.0	0.0	0.0	0.0	0.0	1.0	0.6	0.6	20.9	2.2	2.8	1.6	3.1	1.0	7.8	1.9	320	20.52
NBP9501-17	155–171	5.3 (95-17)	43.1	1.4	2.8	5.6	2.8	0.0	0.0	2.8	1.4	0.0	0.0	0.0	0.0	2.8	4.2	0.0	0.0	4.2	4.2	25.0	0.0	72	5.71 (@ 165 cm)
		CRS mean	41.5	1.7	1.6	4.4	0.8	0.0	0.0	0.3	0.3	0.0	0.4	0.2	0.2	25.7	3.0	0.6	0.9	2.0	1.7	11.8	2.5		15
		CRS SD	13.5	1.9	0.9	3.0	1.0	0.0	0.0	0.8	0.5	0.1	0.4	0.2	0.3	22.4	1.6	1.1	0.8	1.5	1.3	7.5	2.2		9

Note: Point count data for the 500–2000 μm sand-fraction of till. Mineral and lithic fragment percentages have been rounded to the nearest tenth of a percent, therefore the percentages do not always sum to 100% for each sample. SAL numbers correspond to sample numbers assigned in the IUPUI Sediment Analysis Laboratory. In order to demonstrate reproducibity and calculate error, several samples have been counted multiple times. Where this is the case, the average petrographic composition of till from an entire area (i.e. West Antarctica) has been calculated using the average values from the sample replicates. Included with the East Antarctic, West Antarctic, RISP, and several central Ross Sea samples are the original sample numbers as assigned by the original collectors (Dr. Gunter Faure, Dr. James Bockheim, and Dr. Hermand Engelhardt). The reported average particle size for Ross Sea samples 1.5, 2.3, 3.3, and 5.3 are from Licht (1999).

Note: qtz = quartz, pyrox = pyroxene, K-spar = potassium feldspar, plag = palgioclase, cal = calcite, olv = olivine, musc = muscovite, biot = biotite, chlor = chlorite, opq = opaques, unk = unknown, silt = siltstone, s.s. = sandstone, Mudst = mud stone, clayst = claystone, l.s. = limestone, extr = extrusive volcanic, maf = mafic intrusive, int = intermediate intrusive, fel = felsic intrusive, and meta = metamorphic, *n* = number of counts for the thin section, and *d* = the average particle size for the <2000 μm fraction.

well-rounded quartz (58.4±11.0%), felsic intrusive lithic fragments (12.5±3.3%), rounded feldspar (11.8±9.8), and sedimentary lithic fragments (8.4±9.1%) (Fig. 5, Table 3). Many of the felsic intrusive fragments from beneath the Whillans Ice Stream (B) contain feldspar–hornblende–biotite assemblages. A few of the felsic intrusive lithic fragments contain biotite partially replaced by chlorite. Kamb Ice Stream (C) samples contain minor quantities of opaque mineral fragments; whereas opaques are absent from Whillans Ice Stream (B) samples. One of the Kamb Ice Stream (C) samples contains three to four times more plagioclase than the other West Antarctic tills (Table 3). Despite the presence of a large rift basin underlying the West Antarctic ice sheet, samples contain only minor quantities of extrusive lithic fragments and almost no mafic igneous lithic fragments. Overall, West Antarctic samples contain a larger concentration of individual mineral fragments than rock fragments and display less compositional variability between samples than East Antarctic till (Table 3).

5.3. Ross sea

The RISP till samples are from two cores retrieved in very close proximity to one another beneath the Ross Ice Shelf (Fig. 1). In order of decreasing abundance, they contain well-rounded quartz grains (51.9%), sedimentary lithic fragments (mostly mudstone and claystone) (20.9%), and felsic intrusive lithic fragments (16.4%) (Table 3). Mafic intrusive lithic fragments and mafic minerals are nearly absent from RISP samples, but one sample contains over 8% extrusive lithic fragments.

Thirteen WRS samples from six cores were analyzed (Fig. 1, Table 3). Most contain high, but variable concentrations of quartz (45.3±11.9%), mudstone (14.4±11.4%) and mafic intrusive lithic fragments (9.6±3.8%) (Table 3). The sedimentary lithic fragment content in these samples varies widely, from 5.5% to 54.6%. WRS samples also contain mafic minerals, including small amounts of pyroxene and olivine (Fig. 5, Table 3). Small but significant amounts of felsic intrusive lithic fragments, extrusive igneous lithic fragments and subrounded–rounded plagioclase are also present (Table 3).

Seven ERS samples from six cores are dominated by well-rounded quartz (73.4±7.5%), felsic intrusive lithic fragments (8.8±3.7%), and sedimentary lithic fragments (6.9±5.3%) (Fig. 5, Table 3). ERS till samples contain only small concentrations of extrusive lithic fragments (1.3%) and no mafic intrusive lithic fragments. Several felsic intrusive lithic fragments from the ERS contain hornblende and/or alteration of biotite to chlorite (suggesting hydrothermal alteration).

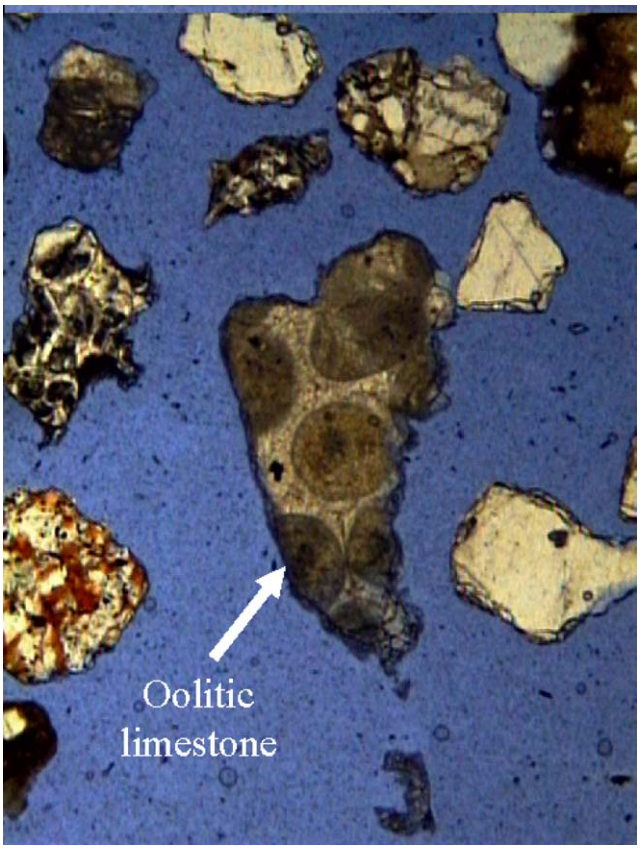

Fig. 4. Photomicrograph of sample SAL 540 magnified 100× under plane-polarized light from core NBP9501-17 in the central Ross Sea highlighting the presence of oolitic limestone.

Eleven samples from six CRS cores are dominated by well-rounded quartz (41.5±13.5%), mudstone (25.7±22.4%), and felsic intrusive lithic fragments (11.8±7.5%) (Fig. 5, Table 3). Small quantities of limestone fragments are present in approximately half of the CRS samples, including a well-preserved oolitic limestone fragment in sample SAL 540 (Fig. 4). Minor mafic lithic and mineral components are also present.

5.4. Ternary diagrams

5.4.1. Quartz-Sedimentary lithic fragment-Mafic intrusive lithic fragment (QSM) ternary diagram

The compositions of East and West Antarctic source terrane till samples plot in distinct areas on the QSM ternary diagram (Fig. 6). East Antarctic till samples contain a wide range of these components and scatter across the $Q = 30-80\%$ area of the ternary. The West Antarctic till samples show less variability and plot along the $Q-S$ axis with >87% quartz. The near absence of mafic intrusive lithic fragments in all West Antarctic till samples contrasts with the more abundant and variable mafic component of the East Antarctic till samples.

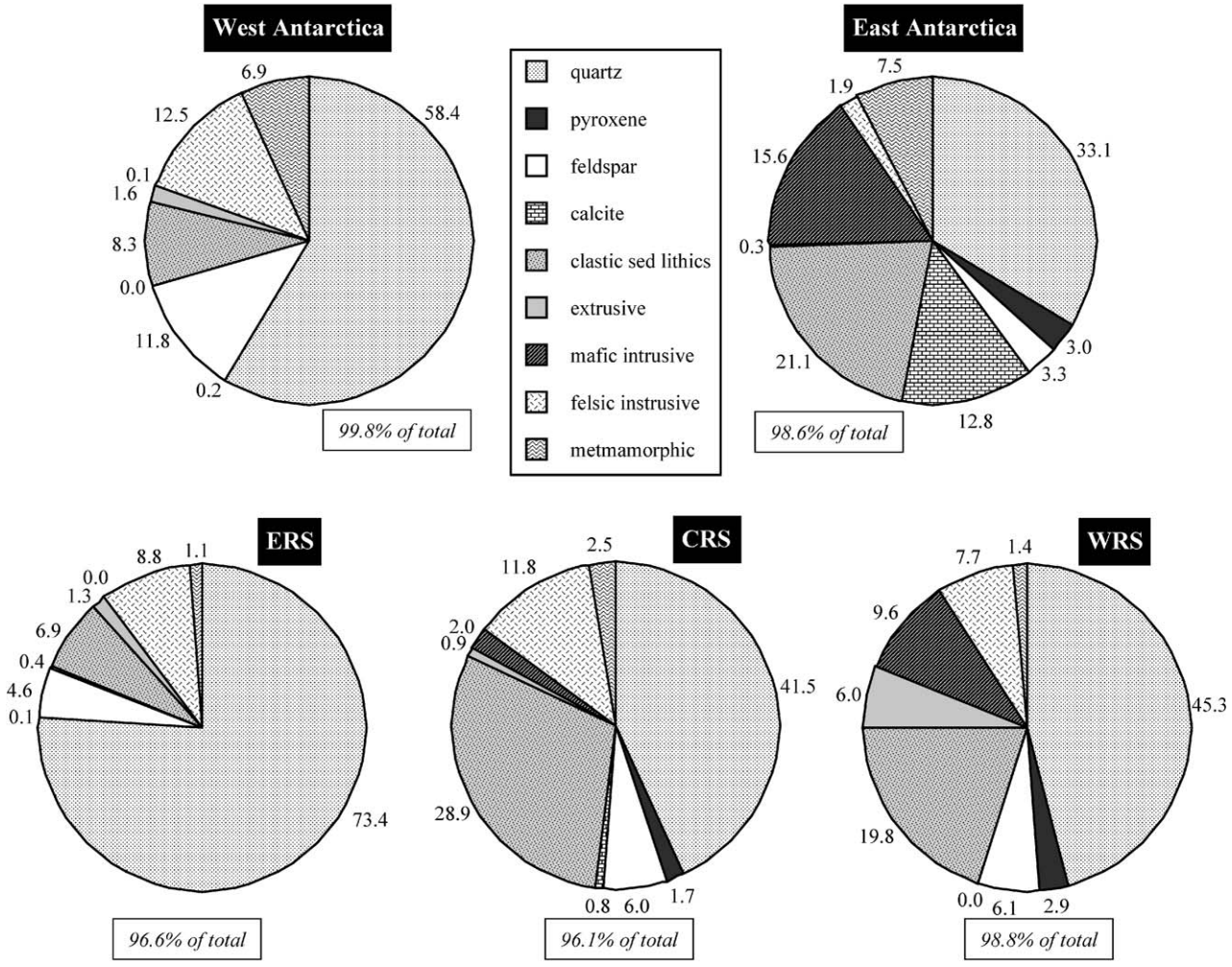

Fig. 5. Pie diagrams showing percentages of major mineralogic and lithologic components of till samples from East and West Antarctica and the Ross Sea. The key lists the components as they appear clockwise in the diagrams. East Antarctic, WRS and CRS till samples contain less quartz, more mafic components and more clastic sedimentary lithic fragments than the West Antarctic and ERS till samples.

Most of the WRS till samples plot within or just beyond the low mafic intrusive lithic fragment portion of the East Antarctic field. The ERS samples are compositionally very similar to the West Antarctic samples as shown by their nearly complete overlap on the QSM diagram. The RISP samples plot close to the $Q-S$ axis with more sedimentary lithic fragments than ERS and West Antarctic samples. Most CRS samples plot between the two source terranes and between the ERS and WRS samples. The QSM plot shows that CRS tills have much higher proportions of sedimentary lithic fragments than their potential West Antarctic source tills.

5.4.2. Quartz-Feldspar-Mafic intrusive lithic fragment (QFM) ternary diagram

Till sample compositions from East and West Antarctica plot in distinct areas on the QFM ternary diagram (Fig. 6). East Antarctic samples plot along the $Q-M$ axis. The only noticeable outlier among East Antarctic till is sample SAL 192 from the Brown Hills, which contains a high proportion of plagioclase and almost no mafic intrusive lithic fragments (Table 3). West Antarctic samples cluster midway along the $Q-F$ axis, highlighting the near absence of mafic intrusive lithic fragments. The majority of the feldspar grains in these West Antarctic till samples are plagioclase (Table 3). RISP samples plot near the Q end-member and overlap with a few East Antarctic samples.

WRS samples contain less mafic intrusive lithic fragments and more feldspar than East Antarctic samples, plotting in an elongate area roughly parallel with the $Q-M$ axis, averaging ~10% feldspar (Table 3). ERS samples all lie along the $Q-F$ axis and are therefore similar to West Antarctic samples although they are more quartz-rich. CRS samples plot between the WRS and the ERS samples. Mafic intrusive lithic fragments are present in most of the CRS samples even

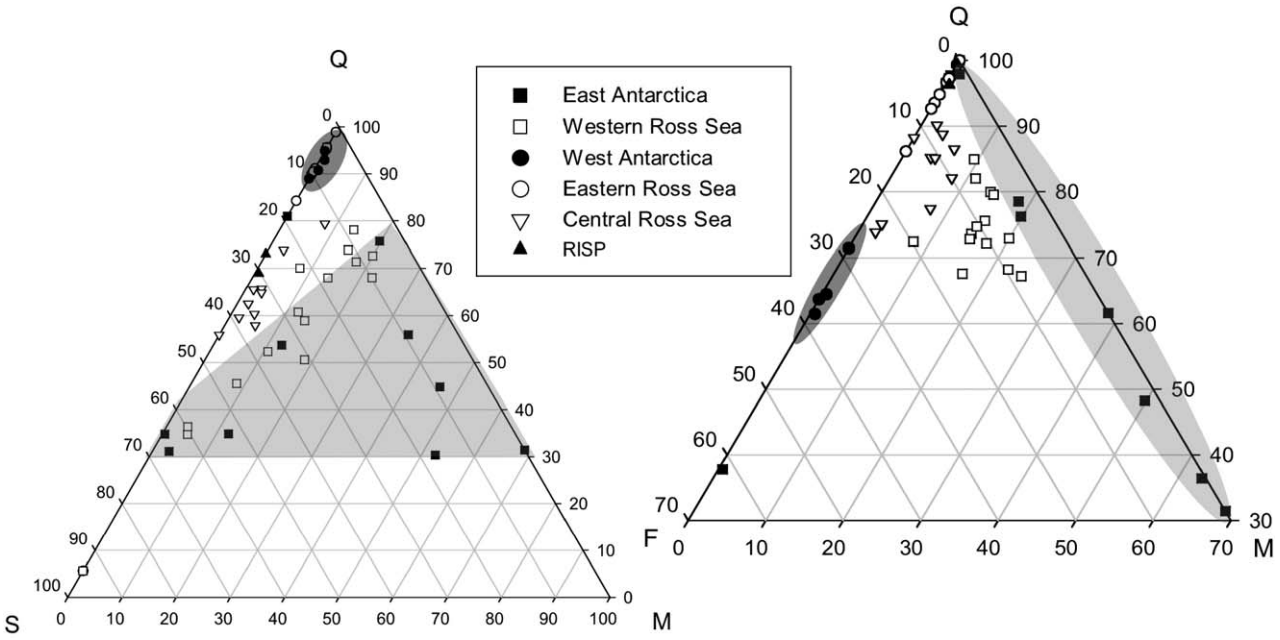

Fig. 6. QSM and QFM ternary plots for the 500–2000 μm sand fraction of all till samples analyzed in this study. The shaded areas highlight positions of the East Antarctic samples (light gray region) and West Antarctic samples (dark gray region). Q = quartz, F = feldspar, M = mafic lithic fragments, S = sedimentary lithic fragments. In order to identify the outliers discussed in the text, the positions of SAL 192 and SAL 227 are indicated. Note that the $Q-F$ and $Q-M$ axes of the QFM ternary are cropped at 70% and 30%, respectively.

though they are virtually absent in the samples from West Antarctica and the ERS.

5.5. Statistical analyses

The results of a cluster analysis provide a statistical correlation of samples based on all of the point count data (except quartz and minerals with abundance $<5\%$). Samples SAL 194 from Lower Byrd Glacier in East Antarctica and SAL 283 from the CRS were eliminated from the final cluster analysis because they did not correlate with any other sample at a Euclidean distance <9.2. SAL 194 comprises predominantly calcite and marble fragments and sample SAL 283 is primarily composed of siltstone lithic fragments.

The dendrogram shows three distinct cluster groups and cluster 2 is further divisible into four, more highly correlated subclusters (Fig. 7). The East Antarctic source terrane samples occur in all three clusters, demonstrating the lack of compositional similarity between these widely distributed samples. Moreover, samples from a single region, such as the Beardmore Glacier, typically do not cluster tightly, reflecting the influence of local rock outcrops on the overall compositional signature. Unlike the more variable East Antarctic tills, all four West Antarctic till samples (cluster 2A) are strongly correlated to each other and link at a Euclidean distance of approximately 3.

This analysis demonstrates that the Ross Sea samples are more similar to each other than they are to the source terrane tills. Within the Ross Sea samples, all ERS points fall into subcluster 2C, indicating their close correlation with each other (Fig. 7). Almost all CRS tills occur in cluster 2B along with the RISP samples. WRS samples show the most compositional diversity of all the Ross Sea samples. Most occur in cluster 2D along with three East Antarctic source terrane samples. The remaining WRS samples occur in clusters 2B and 3 and correlate with CRS and East Antarctic source terrane samples.

Discriminant analysis verifies that all 45 samples were correctly assigned to their respective clusters. The discriminant analysis also shows that all three cluster groups are statistically distinctive (Fig. 8a). Furthermore, all four subclusters in cluster 2 were assigned correctly based on the canonical scores plot (Fig. 8b). The classification functions are not significantly changed by adding the variables excluded from the cluster analysis (i.e., quartz and minerals with abundance $<5\%$), thereby indicating that they are not significant variables in grouping the samples. Discriminant analysis confirms that the methodology used to perform cluster analysis was adequate for grouping the samples.

5.6. Particle size distributions

Detailed analysis shows that East Antarctic sample particle size distributions are the most variable of all the regions and that the WRS sample distributions are most similar to the East Antarctic distributions (Fig. 9).

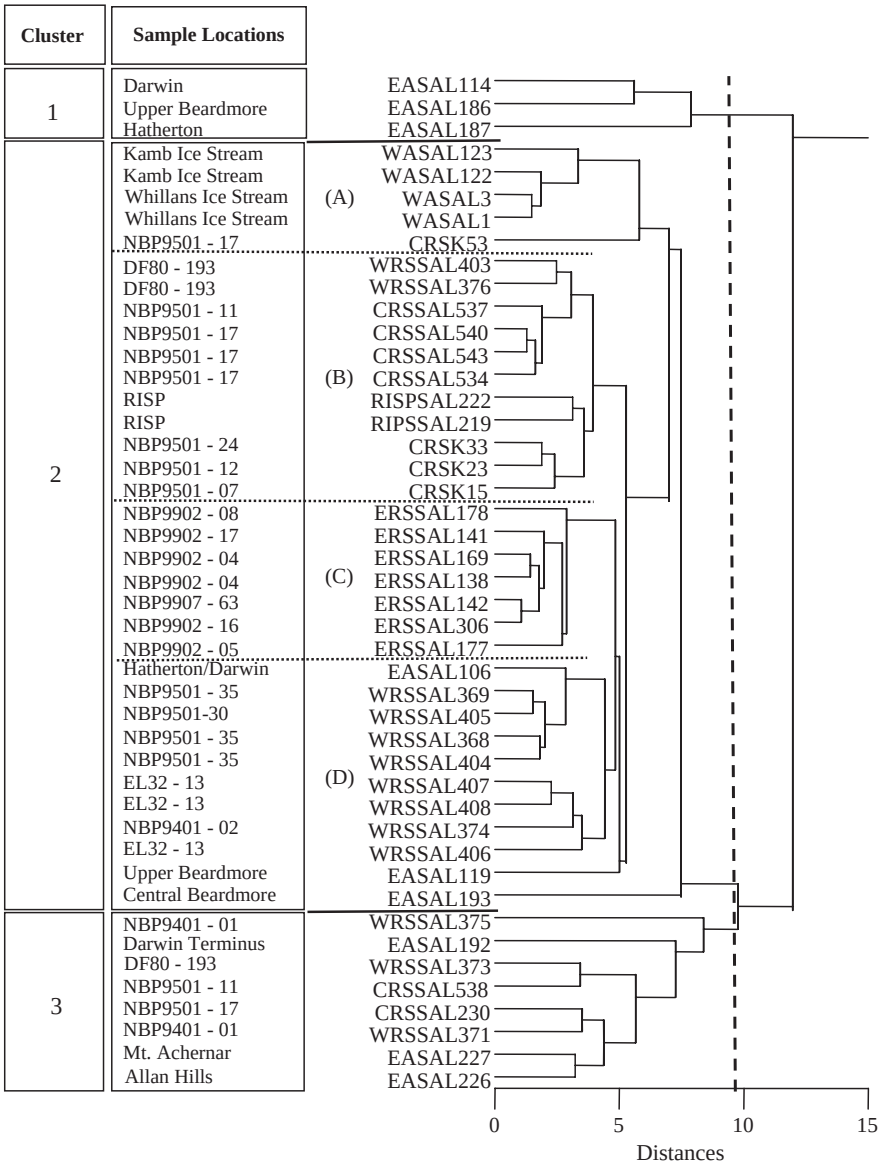

Fig. 7. Cluster tree of all samples analyzed in this study. Three clusters are established at a Euclidean distance of 9.2 delineated by the vertical dashed line. Cluster 2 has been subdivided into four subclusters; A, B, C, and D at a Euclidean distance of ~5.

Overall the CRS, ERS, and RISP particle size distributions are quite similar to each other and more similar to West Antarctic size distributions than to the East Antarctic size distributions.

Results from nine East Antarctic till samples show particle size averages ranging from ~4 to 376 μm (Table 3). Some of these samples have unimodal very fine to fine sand peaks and others have bimodal or trimodal distributions with peaks in the clay to fine silt and sand fractions (Fig. 9a). West Antarctic till sample size distributions from three ice streams (Whillans (B), Kamb (C), and Bindschadler (D)) show less variability than East Antarctic tills (Fig. 9c). Whillans Ice Stream samples have a strong mode at 0.2 μm with additional modes at 7–10, 40, and ~400 μm. One sample from Bindschadler Ice Stream till (SAL 124) is nearly identical to the Whillans Ice Stream samples. Kamb Ice Stream samples are the coarsest of the West Antarctic tills and lack the usual 0.2 μm mode. One Kamb Ice Stream sample (SAL 122) is atypical as it exhibits a strong peak in the very fine sand fraction (~200 μm).

Ross Sea till samples are dominantly composed of silt and clay. Like East Antarctic tills, WRS till samples are characterized by particle size distributions, with a peak in the very fine sand fraction and some with bimodal clay and silt fractions. Although CRS, ERS and RISP samples vary in sand content, all contain distinct modes at 0.2 and 5–10 μm. All but one of the CRS samples contain a small peak at ~150 μm; this signature

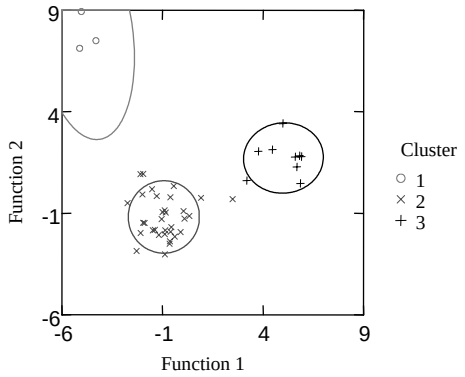

(a)

Function 1:
felsic igneous fragments
Intermediate igneous fragments
extrusive volcanic fragments
opqaue minerals
calcite
potassium feldspar
plagioclase
mudstone fragments
sandstone fragments
claystone fragments

Function 2:
metamorphic igneous fragments
mafic igneous fragments
biotite
iron ore
quartz
olivine
chlorite

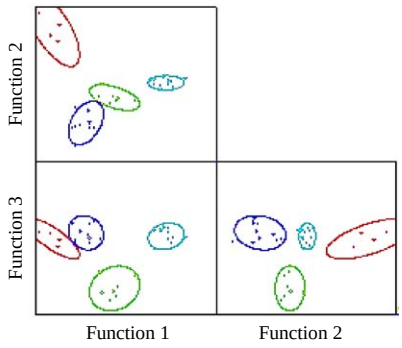

(b)

Function 1:
intermediate igneous fragments
metamorphic fragments
extrusive volcanic fragments
limestone fragments
sandstone/siltstone fragments
claystone fragments
pyroxene
potassium feldspar
biotite
chlorite

Function 2:
mudstone fragments
mafic fragments
felsic fragments
olivine
iron ore
calcite
quartz

Function 3:
opaque minerals
muscovite

Fig. 8. (a) Resulting groups from discriminant analysis exhibit no overlap between groups, confirming that Clusters 1, 2, and 3 are assigned correctly and are distinctly different. Similarly, (b) shows no overlap between groups confirming that the subclusters from Cluster 2 were assigned correctly and are distinctly different. Red = subcluster 2A, light blue = subcluster 2B, green = subcluster 2C, and dark blue = subcluster 2D.

is not apparent in any other Ross Sea samples (Fig. 9e), but does occur in a few East Antarctic samples (Fig. 9a).

6. Discussion and conclusions

The East and West Antarctic till samples, which are the source terranes for the Ross Sea tills, are compositionally distinct and in most cases are consistent with rock types on published maps as summarized in Table 4. East Antarctic till samples are characterized by a wide array of mineral and lithic fragments reflecting the diverse bedrock types throughout the Transantarctic Mountains (Fig. 3). Seventy percent of the East Antarctic samples contain a substantial mafic intrusive lithic component that is likely supplied by rocks of the Ferrar Group and 80% contain clastic sedimentary lithic fragments (mainly mudstone), which are probably derived from the Beacon Supergroup. In a few cases however, the source rock is not readily identifiable. For instance, SAL 187 contains abundant quartzite, however, no mapped metamorphic units occur near or upstream of the sampling location (e.g., see Tingey, 1991), so their source is uncertain. In these cases, it is probable that the source bedrock in the Transantarctic Mountains is ice covered and remains unmapped or that the source is the East Antarctic craton rather than the Transantarctic Mountains.

West Antarctic till samples contain a comparably less diverse mineralogy and lithology than East Antarctic till, with quartz, felsic intrusive lithic fragments, feldspar, sedimentary lithic fragments, and quartzite being the major constituents of the till (Fig. 5). The source of these components is more ambiguous than for the East Antarctic till because of widespread ice cover and the greater distances to mapped bedrock exposures. We infer that the felsic intrusive lithic fragments and plagioclase grains are derived from Granite Harbor Intrusives shed from the Transantarctic Mountains as well as the Byrd Coast Granite and Ford Granodiorite of Marie Byrd Land; the small size of the grains precludes unambiguous identification within these three groups.

Behrendt et al. (1995, 2004) identified West Antarctic mafic volcanic edifices that were likely to have been planed-off by glacial action upstream of the modern ice streams, however, mafic minerals and extrusive lithic fragments are nearly absent from the West Antarctic till (Fig. 5, Table 3). Their absence may indicate that erosion of these features occurred earlier than the LGM and that the sand-sized mafic component may be more common in older Ross Sea till deposits. Thus the absence of the Cenozoic volcanic fragments in the ERS till supports observations of Rooney et al. (1991) that the West Antarctic basin that underlies the West Antarctic ice sheet is filled with up to a kilometer of glacial and marine sediments that mask the rift-related

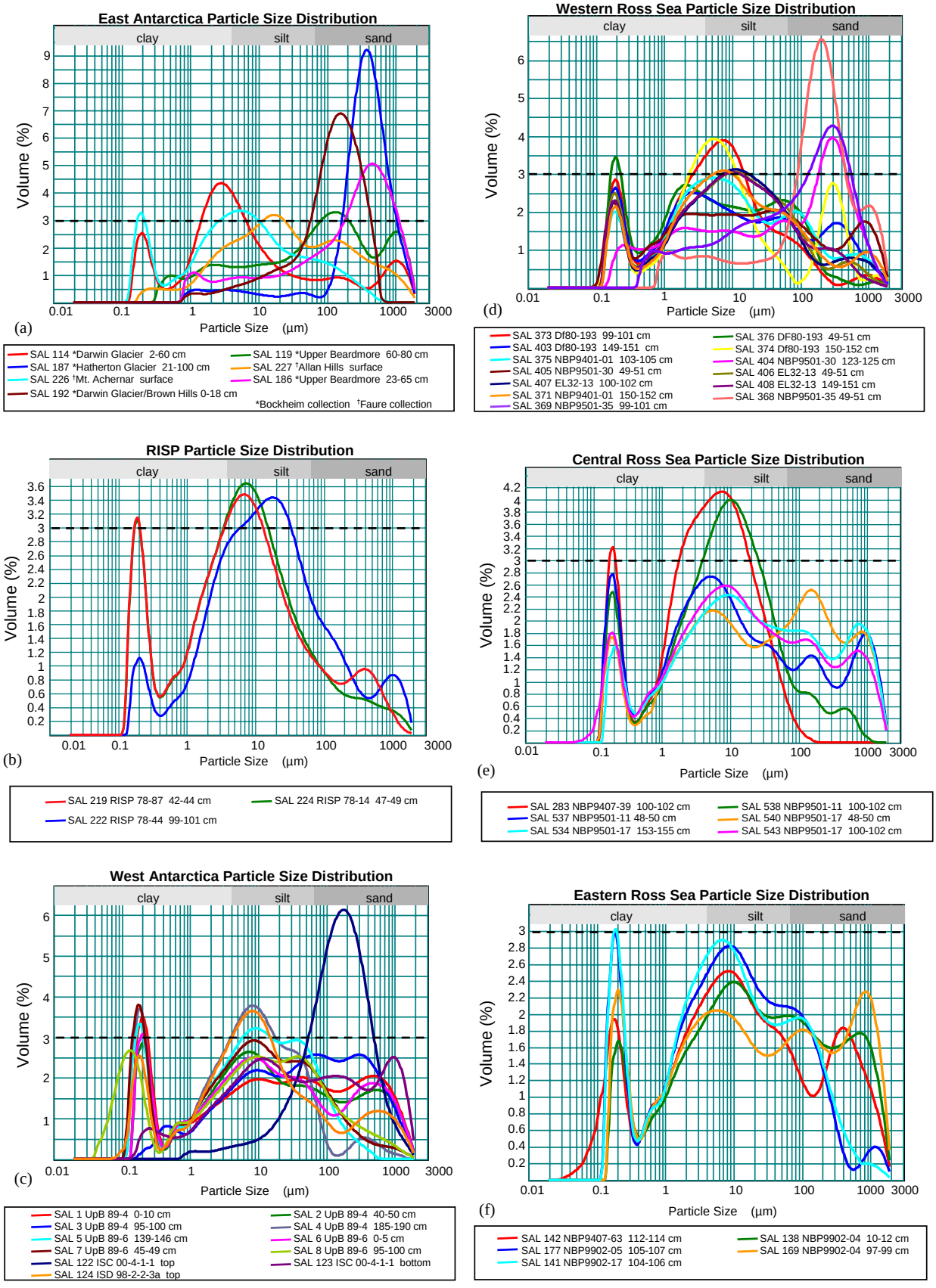

Fig. 9. Particle size analysis distributions for (a) Beardmore Glacier, Mt. Achernar, Byrd Glacier, Darwin Glacier, Hatherton Glacier, Allan Hills, (b) RISP, (c) Whillans Ice Stream (UpB), Kamb Ice Stream (ISC), and Bindschadler Ice Stream (ISD), (d) WRS, (e) CRS, and (f) ERS samples. Because *y* axes are variable, a dashed reference line was drawn at 3%. Data are reported as volume percent.

Table 4
Summary of source till compositions and potential bedrock sources

Sample	Location	Characteristic composition	Potential bedrock sources
East Antarctica			
SAL 106	Hatherton/Darwin (78-14-Cn3)	Mafic intrusive lithics	Ferrar Group
SAL 192	Darwin area/Brown Hills (78-71-Cn1)	Mudstone, plagioclase, felsic intrusive lithics	Beacon Supergroup, Granite Harbor Intrusives
SAL 114	Darwin (78-62-Cn2)	Mafic intrusive lithics, pyroxene, mudstone	Ferrar Group, Beacon Supergroup
SAL 187	Hatherton (78-55-Cn2)	Quartzite, mafic instrusive lithics, felsic intrusive lithics, siltstone/sandstone	Ferrar Group, Beacon Supergroup, Granite Harbor Intrusives
SAL 194	Lower Byrd (78-66-Cn)	Calcite, marble, mafic intrusive lithics	Byrd Group Selbourne Marble, Ferrar Group
SAL 193	Central Beardmore (85-44-Cn2)	Siltstone/sandstone, quartzite	Beardmore Group, Beacon Supergroup
SAL 119	Upper Beardmore (85-44-Cn2)	Mudstone, mafic intrusive lithics, siltstone/sandstone, claystone	Beardmore Group, Beacon Supergroup, Ferrar Group
SAL 186	Upper Beardmore (85-17-Cn2)	Mafic intrusive lithics, pyroxene, quartzite	Ferrar Group, Beacon Supergroup
SAL 226	Mt Achernar	Mudstone, well-rounded quartz grains	Beacon Supergroup
SAL 227	Allan Hills	Mudstone, mafic intrusive lithics	Beacon Supergroup, Ferrar Group
West Antarctica			
SAL 1	Whillans Ice Stream (UpB89-4)	Felsic intrusive lithics, quartzite, mudstone, plagioclase	Granite Harbor Intrusives, Byrd Coast Granite, Ford Granodiorite
SAL 3	Whillans Ice Stream (UpB89-4)	Felsic intrusive lithics, quartzite, plagioclase	
SAL 122	Kamb (00-4-1-1)	Siltstone/sandstone, felsic intrusive lithics, quartzite, plagioclase, extrusive lithic fragments	
SAL 123	Kamb (00-4-1-1)	Plagioclase, felsic intrusive lithics	

Quartz is abundant in all samples, except SAL 194, so it has been omitted here.

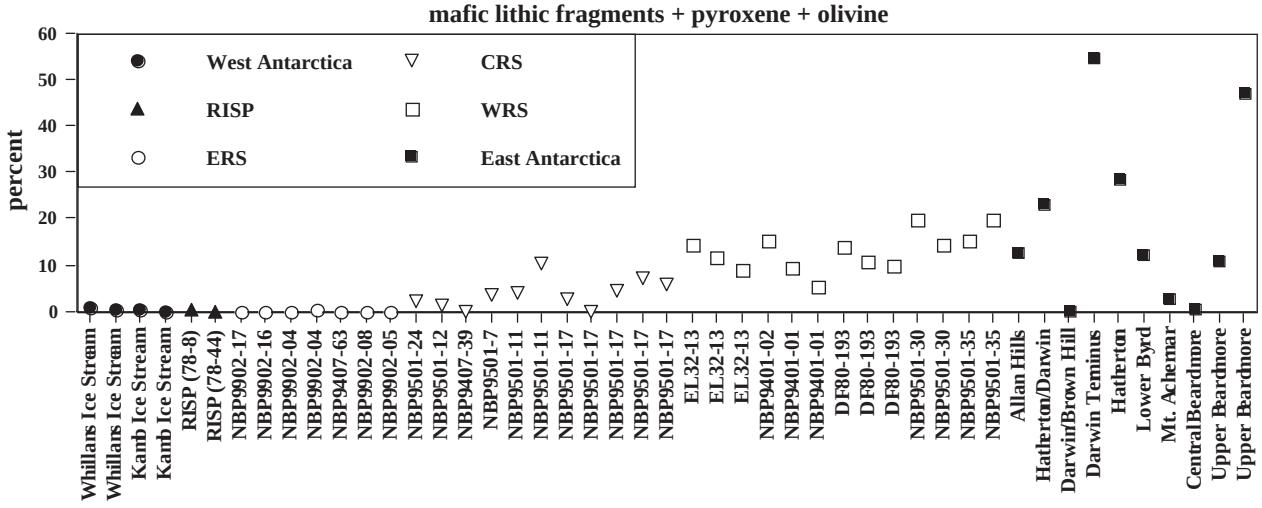

Fig. 10. Percent mafic lithic and mafic mineral components of each sample by region. West Antarctic, RISP and ERS till samples are essentially devoid of a mafic component. Most East Antarctic and WRS till samples contain at least 5% mafics. The intermediate CRS values likely represents the mixing of mafic-bearing East Antarctic till and mafic-poor West Antarctic till.

basalts. The clay fraction of ERS tills shows abundant smectite, which was interpreted to represent altered West Antarctic volcanic rocks delivered by ice streams D and E (Balshaw, 1980). These data suggest that the Cenozoic mafic volcanic rocks may be better represented in the clay-size fraction than the sand-size fraction of West Antarctic-derived till. Overall, based on the samples analyzed in this study, the best distinguishing factor between the sand fraction of East and West Antarctic source terrane tills appears to be the presence or absence of a mafic mineralogic and lithic components (Fig. 10).

6.1. Source terranes and Ross Sea till correlation

All LGM ice-flow models show East Antarctic-derived ice flowing into the WRS. Many reconstructions (e.g., Stuiver et al., 1981) also have West Antarctic ice (particularly the expanded Whillans Ice Stream) contributing to ice in the WRS. Pie charts and ternary diagrams of our data (Figs. 5 and 6), clearly show that WRS till samples are similar in composition to East Antarctic tills. Moreover almost all WRS samples contain the mafic intrusive lithic component characteristic of East Antarctic tills. However, the cluster analysis, which includes almost all the compositional data, does not show strong relationships between East Antarctic and WRS till. This may be related to three factors. First, the greater abundance of extrusive volcanic fragments in WRS till compared to East Antarctic till suggests that rocks of the McMurdo Volcanic Group are incorporated into the ice sheet's basal debris zone after it extends from the Transantarctic Mountains. Based on the location of existing McMurdo Volcanic outcrops, the transport distance of extrusive lithics may range from a few tens of kilometers to over 100 km. Second, in addition to picking up material of a new composition during transport, East Antarctic source terrane till may be modified by crushing and abrasion during transport. The source rocks have a wide range of hardnesses and some ice flow paths may be many hundreds of kilometers long, resulting in comminution of the lithic fragments. A third, and likely possibility, is that East Antarctic and WRS till sample compositions do not always match closely because important source terrane tills are missing from our existing sample collection. For instance, the Nimrod and Scott Glaciers are not represented in our data set and Byrd Glacier is only represented by one sample, which is not necessarily representative of the average Byrd Glacier till composition. However, taken as a whole, the WRS till samples bear strong compositional similarity to East Antarctic till samples and are distinctly different from West Antarctic till samples. These observations are supported by Nd and Sr isotopic analyses of the silt + clay fraction from the same samples (Farmer et al., 2004). WRS samples have substantially higher ε_{Nd} values (−5) than adjacent East Antarctic samples (−12 to −14) because of the incorporation of McMurdo Volcanics which have positive ε_{Nd} values.

The sand fraction of WRS tills analyzed in this study is similar in composition, although more variable, to the sand fraction of Quaternary sediments recovered in the MSSTS-1, CIROS-1 and Cape Roberts Project drill cores (e.g., Barrett et al., 1986; George, 1989; Cape Roberts Science Team, 1998; Smellie et al., 2001). The major reason for the compositional differences is related to the site distances from the coast. All the drill cores were collected within 20 km of the Victoria Land Coast, whereas most of the WRS cores from this study were much further offshore (up to 200 km). Thus the WRS cores contain glacial debris transported from more distant and potentially different source terranes, which may have also been modified during transport through more than one glacial cycle. One additional factor that may contribute to the apparent compositional variability is the difference in point-counting methods (i.e., Gazzi-Dickinson vs. Indiana-method vs. smear slides).

ERS samples are compositionally very similar to the West Antarctic samples. All available West Antarctic till samples plot in a very small field on both ternary diagrams and form the tightest cluster of any region (Fig. 7). Similarly, the cluster analysis and ternary diagrams also show little variability among ERS tills. The ERS samples plot very near or overlap with the West Antarctic data points on both ternary diagrams (Fig. 6). Both the ERS and West Antarctic till samples effectively lack a mafic component (Fig. 10, Table 3). Although the West Antarctic and ERS samples are compositionally similar, ERS tills form their own subcluster (Fig. 7), indicating some consistent differences with the West Antarctic samples. As in the WRS, the difference between ERS till and the West Antarctic source terrane till may be caused by modification of grains during subglacial transport. However Tulaczyk et al. (1998) found little evidence of comminution in the sub-ice stream till indicating this process may be less important during flow over unlithified sediment. Thus the difference in composition between West Antarctic and ERS samples may indicate that rates of comminution have changed through time as basal conditions changed and/or that till beneath the Bindschadler, MacAyeal, and Echelmeyer ice streams has a slightly different composition than the other ice streams. One other possibility is that the ERS till is a mixture formed during multiple ice advances fed from slightly different source terranes. Although we attempted to analyze samples from beneath the Bindschadler ice stream, the sample was too small to obtain enough coarse sand for a statistically significant count. However, Nd and Sr isotopic analyses were performed on the matrix material from the Bindschadler ice stream (Farmer et al., 2004). The Nd and Sr isotopic values are very similar to Whillans ice stream samples, as well as ERS and RISP till samples. Overall, the sand and isotopic compositional data support the expectation of strong similarities between West Antarctic and ERS till samples.

The hypothesis that the CRS represents the location of converging East and West Antarctic ice (Licht and Fastook, 1998; Denton and Hughes, 2000) can be assessed with our data set. On the ternary diagrams, the CRS till sample compositions fall between the WRS and ERS compositional fields, suggesting that the CRS till may represent a mixture of East and West Antarctic sources. Furthermore, most CRS till samples contain

mafic intrusive lithic and mafic mineral components, which are observed almost exclusively in the WRS and East Antarctic till samples (Fig. 10, Table 3). The values are lower than the WRS and East Antarctic tills, suggesting a mixture of mafic-free West Antarctic-derived till and mafic-bearing East Antarctic-derived till. An East Antarctic source for CRS till is also indicated by the presence of an oolitic limestone fragment in one CRS sample (Fig. 4). Oolitic limestone has only been mapped in rocks of the Holyoake Range near the Nimrod Glacier, which bisects the Transantarctic Mountains (Fig. 3). Additionally, Nd and Sr analyses from CRS cores show low ε_{Nd} values (−9.5 to −12), indicative of an East Antarctic source terrane (Farmer et al., 2004). The cluster analysis shows the closest correlations of CRS till to WRS and RISP samples. One CRS sample, however, clusters with West Antarctic till. All of the analyses support one conclusion, that the confluence of the East and West Antarctic ice sheets occurred in the CRS during the LGM.

6.2. Particle-size analysis

Particle-size analysis may be used to shed some light on the process of till maturation during transport. Dreimanis and Vagners (1969) found that till deposited subglacially matures with transport distance, causing matrix modes to grow. If comminution was occurring at the base of the ice sheet, Ross Sea till should have a finer grain size than the source terrane tills. However, this may be complicated by the incorporation of fine-grained marine sediments during ice advance, as well as the possibility that minerals have reached a characteristic terminal size during subglacial modification (Dreimanis and Vagners, 1969). If the source terrane tills are near this terminal grade, little change in particle size may be observed. This may be the case for the West Antarctic and ERS till samples. Fig. 9 shows little difference in the particle size distributions between these regions. West Antarctic till samples (minus one Kamb Ice Stream outlier) average 73.4% silt + clay and ERS till samples average 71.1% silt + clay. These similarities may support the observation that comminution is not an active process at the base of the West Antarctic ice sheet (Tulaczyk et al., 1998). If a substantial amount of marine silt and clay (Domack et al., 1999; Licht et al., 1999) was incorporated into the till as grounded ice advanced, the ERS till should be finer-grained than West Antarctic till; this trend is not apparent. These data suggest that the compositional variability is not associated with substantial particle size changes, but may be a function of the limited samples from the beneath the West Antarctic ice sheet.

Identifying the relationship between East Antarctic and WRS particle size distributions is complicated by a wide range of starting particle size distributions in East Antarctic till samples (Fig. 9). Because the samples were collected close to bedrock outcrops, the coarse nature of some of the East Antarctic tills is not surprising. The average silt + clay content of East Antarctic till samples is 41.8%, whereas WRS till samples average 70.4% silt + clay, suggesting substantial comminution of the till and also perhaps incorporation of fine-grained marine sediment during ice sheet advance. These disparate particle size distributions may explain some of the observed sand composition variability.

Particle size analyses from this study show that West Antarctic subglacial till samples generally contain finer material than East Antarctic till samples collected from lateral moraines (Fig. 9, Table 3). This is consistent with Tulaczyk et al. (1998), who compared Whillans Ice Stream till with till from Mackay Glacier and Taylor Glacier in East Antarctica, concluding that West Antarctic till samples have a finer particle-size than East Antarctic samples largely because they are a secondary deposit and have been reworked subglacially. Rooney et al. (1991) suggested that West Antarctic tills are probably derived from preexisting Tertiary glacimarine sediments of the Ross Sequence.

6.3. LGM paleoice-flow reconstruction

The distinct compositions of East and West Antarctic till samples combined with the similarities of ERS and WRS till samples with their adjacent land areas provide important constraints on paleo ice-flow paths. Although a highly detailed LGM flow-line reconstruction is not possible because of the low sample density and the complexities introduced by multiple ice advances across the continental shelf, these data demonstrate that determining till provenance in Antarctica is possible and provide the basis for generating LGM ice-flow lines for the Ross Embayment.

The composition of CRS till is crucial in delineating the relative extent of the ice derived from East and West Antarctica in the Ross Sea, which has important implications for Siple Coast ice stream history. CRS samples contain large concentrations of sedimentary lithic fragments (including oolitic limestone) and smaller, but significant amounts of mafic intrusive lithic fragments indicating a strong contribution from an East Antarctic source. Several CRS samples also contain features indicative of a West Antarctic source, including felsic intrusive lithic fragments with hornblende and evidence of hydrothermal alteration of biotite to chlorite (similar to grains observed in West Antarctic till samples). Because the CRS till samples contain sand with compositional similarities to both ERS and WRS samples, we conclude that the CRS represents the confluence of West Antarctic- and East Antarctic-derived ice. Fig. 11 shows a simple reconstruction of LGM ice-flow based on our provenance results.

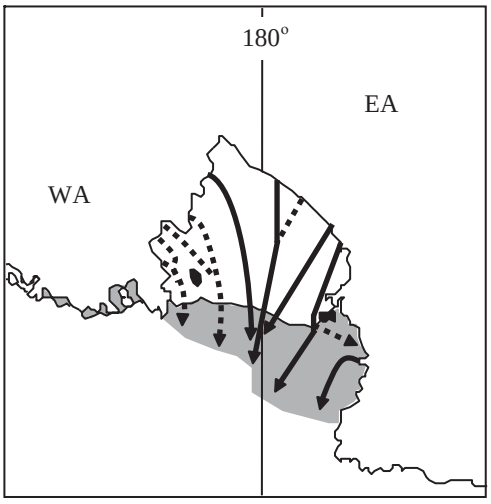

Fig. 11. Proposed flow lines for the Ross Ice Sheet during the LGM based on Ross Sea, and East and West Antarctic till mineralogy and lithology. Dashed lines represent inferred flow due to lack of sample coverage.

The presence of East Antarctic-derived ice in the CRS indicated by these provenance data necessarily implies a substantial change in the Siple Coast ice streams during the LGM. West Antarctic ice appears to have been confined to the three seafloor troughs in the eastern and central Ross Sea. Therefore, if the Siple Coast ice streams were persistent features in the ice sheet, some must have merged together to stay confined to the troughs. Abundant NE–SW trending mega-scale glacial lineations (Shipp et al., 1999) and clear till fabric in sediment cores (Licht, 1999) provide evidence of substantial subglacial deformation of CRS till by streaming ice, which our data indicate formed at the confluence of East- and West Antarctic-derived ice. The presence of streaming ice in the CRS is supported by modeling results of Licht and Fastook (1998) and Fastook and Johnson (2003). Any ice streams that may have been present in the WRS must have been supplied by East Antarctic-derived ice and were not extensions of the Siple Coast ice streams.

Overall, the LGM ice-flow lines for the Ross Ice Sheet indicated by the sand petrologic data are consistent with the models proposed by Licht and Fastook (1998) and Denton and Hughes (2000). Their models show that LGM ice advanced onto the Ross Sea continental shelf, receiving a more equal contribution from East and West Antarctica than had been previously suggested (e.g., Stuiver et al., 1981). Interestingly, the LGM paleo ice-flow reconstruction of Denton and Hughes (2000) shows that the Nimrod Glacier would have extended into the CRS, which is consistent with the presence of oolitic limestone in CRS till.

Assuming our provenance data accurately reflects the confluence of the East and West Antarctic ice sheets in the CRS, then pre-LGM equivalents of the Siple Coast ice streams did not simply extend to form a West Antarctic-dominated ice sheet in the Ross Embayment during the LGM. Although provenance data cannot directly constrain ice flow rates during the LGM, these data do provide important information on the configuration of the Ross Ice Sheet, thus aiding modelers in the construction of more reliable LGM Antarctic ice-flow paths and leading to a greater understanding of the controls on Antarctic ice sheet behavior.

Acknowledgments

This research was supported by a grant from NSF-OPP to Indiana University–Purdue University Indianapolis (OPP-0003600) and from a GSA Graduate Student Grant 7192-02. We are grateful to H. Engelhardt, J. Bockheim, G. Faure, as well as INSTAAR at the University of Colorado and the Antarctic Research Facility at Florida State University for generously supplying samples used in this study. We thank Andy Barth for helpful discussions, along with S. Hicock and an anonymous reviewer for constructive comments.

References

Anderson, J.B., 1999. Antarctic Marine Geology. Cambridge University Press, New York 289pp.

Anderson, J.B., Shipp, S.S., Bartek, L.R., Reid, D.E., 1992. Evidence for a grounded ice sheet on the Ross Sea continental shelf during the Late Pleistocene and preliminary paleodrainage reconstruction. Marine Geology 57, 295–333.

Anderson, J.B., Shipp, S.S., Lowe, A.L., Wellner, J.S., Mosola, A.B., 2002. The Antarctic Ice Sheet during the Last Glacial Maximum and its subsequent retreat history: a review. Quaternary Science Reviews 21, 49–70.

Andrews, J.T., 2000. Icebergs and iceberg rafted detritus (IRD) in the North Atlantic: facts and assumptions. Oceanography 13, 100–108.

Balshaw, K.M., 1980. Antarctic glacial chronology reflected in the Oligocene through Pliocene sedimentary section in the Ross Sea. Ph.D. Thesis, Rice University, 140pp.

Barrett, P.J., 1991. The Devonian to Jurassic Beacon Supergroup of the Transantarctic Mountains and correlatives in other parts of Antarctica. In: Tingey, R.J. (Ed.), The Geology of Antarctica. Oxford University Press, New York, pp. 120–152.

Barrett, P.J., McKelvey, B.C., Walker, B.C., 1986. Sand provenance. In: Barret, P.J. (Ed.), Antarctic Cenozoic History from the MSSTS-1 Drillhole. DSIR Bulletin 237. DSIR Publishing, Wellington, pp. 137–144.

Behrendt, J.C., Cooper, A.K., 1991. Evidence of rapid Cenozoic uplift of the shoulder escarpment of the West Antarctic rift system and a speculation on possible climate forcing. Geology 19, 315–319.

Behrendt, J.C., Le Masurier, W.E., Cooper, A.K., Tessenohn, F., Trehu, A., Damaske, D., 1991. The West Antarctic Rift System—a review of geophysical investigations, American Geophysical Union Antarctic Research Series, vol. 53. American Geophysical Union, Washington, DC, pp. 67-112.

Behrendt, J.C., Blankenship, D.D., Finn, C.C., Bell, R.E., Sweeney, R.E., Hodge, S.M., Brozena, J.M., 1994. CASERTZ aeromagnetic

data reveal late Cenozoic flood basalts (?) in the West Antarctic rift system. Geology 22, 527–530.

Behrendt, J.C., Blankenship, D.D., Damaske, D., Cooper, A.K., 1995. Glacial removal of late Cenozoic subglacially emplaced volcanic edifices by the West Antarctic ice sheet. Geology 23, 1111–1114.

Behrendt, J.C., Blankenship, D.D., Morse, D.L., Bell, R.E., 2004. Shallow-source aeromagnetic anomalies observed over the West Antarctic Ice Sheet compared with coincident bed topography from radar ice sounding—new evidence for glacial "removal" of subglacially erupted late Cenozoic rift-related volcanic edifices. Global and Planetary Change 42, 177–193.

Bentley, C.R., 1991. Configuration and structure of the subglacial crust. In: Tingey, R.J. (Ed.), The Geology of Antarctica. Oxford University Press, New York, pp. 1077–1078.

Bushnell, V.C., Craddock, C. (Eds.), 1970. Antarctic Map Folio Series. American Geographical Society, New York Map 64–29.

Cape Roberts Science Team, 1998. Quaternary strata in CRP-1, Cape Roberts Project, Antarctica. Terra Antarctica 5, 31–61.

Dalziel, I.W.D., Lawver, L.A., 2001. The lithospheric setting of the West Antarctic ice sheet. In: Alley, R.B., Bindschadler, R.A. (Eds.), The West Antarctic Ice Sheet, Behavior and Environment. Antarctic Research Series, Vol. 77, pp. 29–44.

Davis, J.C., 1986. Statistics and Data Analysis in Geology, second edition. Wiley, New York 646pp.

Denton, G.H., Hughes, T.J., 2000. Reconstruction of the Ross Ice Drainage System, Antarctica, at the Last Glacial Maximum. Geografiska Annaler 2–3 (82A), 143–166.

Dickinson, W.R., 1970. Interpreting detrital modes of graywacke and arkose. Journal of Sedimentary Petrology 40, 695–707.

Domack, E.W., Jacobson, E.A., Shipp, S.S., Anderson, J.B., 1999. Sedimentologic and stratigraphic signature of the Late Pleistocene/Holocene fluctuation of the West Antarctic Ice Sheet in the Ross Sea: a new perspective, Part 2. Geological Society of America Bulletin 111, 1517–1536.

Dreimanis, A., Vagners, U.J., 1969. Lithologic relation of till to bedrock. In: Wright, H.E. (Ed.), Quaternary Geology and Climate. National Academy of Sciences, Washington, pp. 93–98.

Drewry, D.J. (Ed.), 1983. Antarctica: Glaciological and Geophysical folio. Cambridge University Press, Cambridge Scott Polar Research Institute.

Fastook, J.L., Johnson, J.V., 2003. Ten years development on UMISM: application to advance and retreat of the Siple Coast Region. West Antarctic Ice Sheet Initative, Tenth Annual Workshop Agenda and Abstracts, Algonkian Meeting Center, Sterling, VA, pp. 42–43.

Fitzgerald, P.G., 1992. The Transantarctic Mountains of Southern Victoria Land: the application of apatite fission track analysis to a rift shoulder uplift. Tectonics 11, 634–662.

Gazzi, P., 1966. Le arenaire del flysch sopracretaceo dell'Appenni no modenese; correlazioni con il flysch di Monghidoro. Mineralogica et Petrographica Acta 12, 69–97.

George, A., 1989. Sand provenance. In: Barret, P.J. (Ed.), Antarctic Cenozoic History from the CIROS-1 Drillhole, McMurdo Sound. DSIR Bulletin 245. DSIR Publishing, Wellington, pp. 159–167.

Goodge, J.W., Fanning, C.M., 1999. 2.5 b.y. of punctuated Earth history as recorded in a single rock. Geology 27 (11), 1007–1010.

Goodge, J.W., Hansen, V.L., Peacock, S.M., Smith, B.K., Walker, N.W., 1993. Kinematic evolution of the Miller Range shear zone, central Transantarctic Mountains. Tectonics 12, 1460–1478.

Goodge, J.W., Myrow, P., Williams, I.S., Bowring, S., 2002. Age and provenance of the Beardmore Group, Antarctica: constraints on Rodinia supercontinent breakup. Journal of Geology 110, 393–406.

Hall, B.L., Denton, G.H., 1999. New relative sea-level curves for the southern Scott Coast, Antarctica: evidence for Holocene deglaciation of the western Ross Sea. Journal of Quaternary Science 14, 641–650.

Hughes, T.J., 1973. Is the West Antarctic Ice Sheet disintegrating? Journal of Geophysical Research 78, 7884–7909.

Hughes, T.J., 1977. West Antarctic ice streams. Reviews of Geophysics and Space Physics 15, 1–46.

Jankowski, E.J., Drewry, D.J., 1981. The structure of West Antarctica from geophysical studies. Nature 291, 17–21.

Kellogg, T.B., Truesdale, R.S., Osterman, L.E., 1979. Late Quaternary extent of the West Antarctic ice sheet: new evidence from Ross Sea cores. Geology 7, 249–253.

Kyle, P.R., 1990. McMurdo volcanic group western Ross Embayment. In: Le Masurier, W.E., Thomson, J.W. (Eds.), Volcanoes of the Antarctic Plate and Southern Oceans. American Geophysical Union, Washington, DC, pp. 48–80.

Laird, M.G., Mansergh, G.H., Chappell, J.M.A., 1971. Geology of the central Nimrod Glacier Area, Antarctica. New Zealand Journal of Geology and Geophysics 14, 427–468.

Lawver, L.A., Royer, J.Y., Sandwell, D.T., Scotse, C.R., 1991. Evolution of the Antarctic continental margin. In: Thomson, M.R.A., et al. (Eds.), Geological Evolution of Antarctica. Cambridge University Press, Cambridge, UK, pp. 533–540.

Le Masurier, W.E., 1990. Late Cenozoic volcanism on the Antarctic plate—an overview. In: Le Masurier, W.E., Thomson, J.W. (Eds.), Volcanoes of the Antarctic Plate and Southern Oceans. American Geophysical Union Antarctic Research Series, Vol. 48, American Geophysical Union, Washington, DC, pp. 1–19.

Le Masurier, W.E., Rex, D.C., 1991. The Marie Byrd land volcanic province and its relation to the cenozoic West Antarctic rift system. In: Tingey, R.J. (Ed.), The Geology of Antarctica. Oxford University Press, New York, pp. 249–284.

Le Masurier, W.E., Wade, F.A., 1976. Volcanic history in Marie Byrd Land: implications with regard to southern hemisphere tectonic reconstructions. In: González-Farrán, O. (Ed.), Proceedings of the International Symposium on Andean and Antarctic Volcanology Problems. IAVCEI, Rome, pp. 398–424.

Licht, K.J., 1999. Investigations into the Late Quaternary history of the Ross Sea, Antarctica. Ph.D. Thesis, University of Colorado, Boulder, 234pp.

Licht, K.J., 2004. The Ross Sea's contribution to eustatic sea level during meltwater pulse 1A. Sedimentary Geology 165, 343–353.

Licht, K.J., Andrews, J.T., 2002. The ^{14}C record of Late Pleistocene ice advance and retreat in the central Ross Sea, Antarctica. Arctic, Antarctic, and Alpine Research 34, 324–333.

Licht, K.J., Fastook, J., 1998. Constraining a numerical ice sheet model with geologic data over one ice sheet advance/retreat cycle in the Ross Sea. Chapman Conference on the West Antarctic Ice Sheet, University of Maine, 25–26.

Licht, K.M., Jennings, A.E., Andrews, J.T., Williams, K.M., 1996. Chronology of the Late Wisconsin ice retreat from the western Ross Sea, Antarctica. Geology 24, 223–226.

Licht, K.J., Dunbar, N.W., Andrews, J.T., Jennings, A.E., 1999. Distinguishing subglacial till and glacial marine diamictons in the western Ross Sea, Antarctica: implications for a Last Glacial Maximum grounding line. Geological Society of America Bulletin 111, 91–103.

Luyendyk, B.P., Richard, S.M., Smith, C.H., Kimbrough, D.L., 1991. Geological and geophysical investigations in the northern Ford Ranges, Marie Byrd Land, West Antarctica. In: Yoshida, Y., Kaminuma, K., Shiraishi, K. (Eds.), Recent Progress in Antarctic Earth Science. Terra Sci., Tokyo, pp. 279–288.

Myrow, P.M., Pope, M.C., Goodge, J.W., Fischer, W., Palmer, A.R., 2002. Depositional history of pre-Devonian strata and timing of Ross Orogenic tectonism in the central Transantarctic Mountains, Antarctica. Geological Society of America Bulletin 114, 1070–1088.

Rooney, S.T., Blankenship, D.D., Alley, R.B., Bentley, C.R., 1991. Seismic reflection profiling of a sediment-filled graben beneath ice stream B, West Antarctica. In: Thomson, M.R.A., Crame, J.A.,

Thomson, J.W. (Eds.), Geological Evolution of Antarctica. Cambridge University Press, New York, pp. 261–265.

Scherer, R.P., Aldahan, A., Tulaczyk, S., Possnert, G., Engelhardt, H., Kamb, B., 1998. Pleistocene collapse of the West Antarctic Ice Sheet. Science 281, 82–85.

Shipp, S.S., Anderson, J.B., Domack, E.W., 1999. Seismic signature of the Late Pleistocene fluctuation of the West Antarctic Ice Sheet system in the Ross Sea: a new perspective, Part 1. Geological Society of America Bulletin 111, 1486–1516.

Smellie, J.L., Ehrmann, W., Talarico, F. (Eds.), 2001. Studies from the Cape Roberts Project, Ross Sea, Antarctica; scientific report of CRP-3; Part II, provenance and climate from petrological studies for CRP-3, Terra Antartica 8, 445–582.

Sneath, P.H.A., 1977. A method for testing the distinctness of clusters; a test of the disjunction of two clusters in Euclidean space as measured by their overlap. Journal of the International Association for Mathematical Geology 9, 123–143.

Stuiver, M., Denton, G.H., Hughes, T.J., Fastook, J.L., 1981. History of the marine ice sheets in West Antarctica during the last glaciation: a working hypothesis. In: Denton, G.H., Hughes, T.J. (Eds.), The Last Great Ice Sheets. Wiley-Interscience, New York, pp. 319–439.

Stump, E., 1995. The Ross Orogen of the Transantarctic Mountains. Cambridge University Press, Cambridge 284pp.

Suttner, L.J., 1974. Sedimentary petrographic provinces: an evaluation. In: Ross, C.A. (Ed.), Paleogeographic Provinces and Provinciality. SEPM Special Publication, Vol. 21, pp. 75–84.

Suttner, L.J., Basu, A., Mack, G.H., 1981. Climate and the origin of quartz arenites. Journal of Sedimentary Petrology 51, 1235–1246.

Systat 8.0, 1998. SPSS, Inc., Chicago.

Tingey, R.J. (Ed.), 1991. The Geology of Antarctica. Oxford University Press, New York 680pp.

Tulaczyk, S., Kamb, B., Scherer, R.P., Engelhardt, H.F., 1998. Sedimentary processes at the base of a West Antarctic ice stream: constraints from textural and compositional properties of subglacial debris. Journal of Sedimentary Research 68, 487–496.

Weaver, S.D., Bradshaw, J.D., Adams, C.J., 1991. Granitoids of the Ford Ranges, Marie Byrd Land, Antarctica. In: Thomson, M.R.A., et al. (Eds.), Geological Evolution of Antarctica. Cambridge University Press, Cambridge, UK, pp. 345–351.

Wilson, T.J., 1992. Mesozoic and Cenozoic kinematic evolution of the Transantarctic Mountains. In: Kaminuma, K., Toshida, Y. (Eds.), Recent Progress in Antarctic Earth Science. Terra, Tokyo, pp. 303–314.